nature portfolio

Peer Review File

Multimodal spatial transcriptomic characterization of mouse kidney injury and repair

Corresponding Author: Dr Benjamin Humphreys

This file contains all reviewer reports in order by version, followed by all author rebuttals in order by version.

Attachments originally included by the reviewers as part of their assessment can be found at the end of this file.

Version 0:

Reviewer comments:

Reviewer #1

(Remarks to the Author)
In this manuscript Xuanyuan et al. present a dataset of Visium and Xenium spatial transcriptomics along the timeline of progression of IRI. The authors present an interesting analisys of the combined data through registration of the sequential sections. The authors make a commendable job of making the data available, including a platform in the lab webpage that allows interactive exploration of the combined dataset. As the authors clearly stated, such a dataset is of fundamental importance to evaluate computational methods such as cell type deconvolution, which is particularly challenging in an organ such as the kidney.

I believe the codes could be more comprehensive regarding the analysis performed in the interest of reproducibility. For instance, there is no script guiding the reader on how to perform the expression imputation. Several scripts on zenodo to generate figures require the analyzed object. There is a github page presenting some of the analysis, but more scripts for this particular manuscript could be made available.

A xenium dataset with celular resolution and spatial localization has the potential to be a unique tool to investigate cell cell communication. However, I believe this could significantly be improved on this manuscript. Particularly the results presented on figure 6A. As stated on the main text the authors "integrated reference snRNA-seq data to infer spatially resolved cell-cell communications". This could be rewritten to make clear the expression is imputated for this analysis. It is present on the methods, but it is important enough to warrant a place on the main manuscript. Particularly because some of the communication presented is contradicted by the spatial data generated in this work. For instance, Sema3c is not present on Xenium, while in visium is found on the urothelium;
Nrg1 is found on FR_PT on xenium, but its ligand only in urothelium in visium; the receptor Bmpr2 is present in endothelial cells on the xenium dataset; Csf1 is not found in FR_PT in xenium nor viusim; among other examples.

Regarding novelty, the authors provide a rich dataset characterizing a model of acute kidney injury. The xenium dataset is of particular value, as it may also guide the panel selection of future studies. I would also like the authors to better contextualize how the findings in this paper characterizing the failed repair proximal tubule, and some of the identified communication, such as Ccl2 or Csf1, add to the previous description of this model by the lab on Muto et al.

Overall, I believe this manuscript is well written, and the generated dataset is valuable to the community.

(Remarks on code availability)
There is no code that reproduces the results. There is a github page with some similar examples, and the code available in zenodo generates displays based on processed data.

Reviewer #2

(Remarks to the Author)
The manuscript "Multimodal Spatial Transcriptomic Characterization of Mouse Kidney Injury and Repair" by Xuanyuan et al.

presents a detailed spatial analysis of acute kidney injury (AKI) using bilaterial IRI mouse model, employing two complementary technologies: Xenium and Visium. The study analyzes 12 mouse kidneys across six stages of disease progression, focusing on dynamic changes in spatial cellular neighborhoods that cannot be captured with single-cell RNA sequencing alone. Notably, the study highlights failed-repair proximal tubular cells (FR-PTC), which form unique niches with fibroblasts and immune cells.
While the data quality is high and the findings are insightful, the study could benefit from further exploration of biological insights. Recent spatial datasets, such as Polonsky et al. using SeqFISH+ in Nature Communications, targeted 1,300 genes but analyzed only a single time point (day 28). The distinctiveness of this manuscript lies in its integration with Visium, a full-transcriptome spatial assay from the same section, allowing for a more comprehensive temporal analysis.
However, the manuscript currently mixes data description with benchmarking of spatial software tools, which detracts from the focus on biological insights, which are currently underexplored. A clearer narrative on the biological implications is needed. Below are key points that require attention:
1. Sample Size and Sex Differences: The sample size of n=2 per time point is too low, particularly for analyzing sex-specific differences. Including tissues from models treated with antifibrotic drugs (e.g., Finerenone or SGLT2 inhibitors) could provide additional insights.
2. Cell Type Composition and Validation: The comparison of cell-type compositions between spatial transcriptomics and single-cell data should be further validated, potentially at the protein level. Deconvolution of the Visium data should confirm observed cell-type changes, yet these findings currently add little to the biological narrative.
3. Cell Neighborhood Analysis: The rationale for the chosen the described spatial neighborhood approach needs elaboration. Tools like CellCharter or NichePCA could offer a more robust analysis of spatial domains and their temporal dynamics. Clarifying why these specific approaches were chosen over others would strengthen the methodological transparency.
4. Benchmarking Deconvolution Methods: Although the benchmarking of deconvolution tools is informative, it diverts from the manuscript's main biological focus. Integrating deeper biological analysis would strengthen the study. The emphasis on tool performance over biological discovery can distract readers from the core findings.
5. Spatial Data Integration: The manuscript describes a binning approach to integrate Visium and Xenium data, involving manual adjustments to achieve shared cellular compositions. This method could introduce biases, and alternative approaches should be considered. A quantitative assessment of how this manual integration impacts results would be beneficial.
6. Receptor-Ligand Interactions: The current analysis using CellChat lacks dynamic exploration of cell-cell communication (CCC). NicheNet could provide a more comprehensive modeling of intercellular communication, especially given the time-course nature of the data. The authors should aim to link CCC findings to specific biological outcomes, such as fibrosis predisposition within certain tissue niches.
7. Limited Exploration of Longitudinal Changes: Although the study spans multiple time points, the temporal dynamics of key molecular and cellular interactions are underexplored. Highlighting changes in receptor-ligand interactions or shifts in cell state populations over time would add valuable context to the findings.
8. Biological Validation: The study relies heavily on computational predictions without sufficient experimental validation. Functional assays, such as knockdown or overexpression studies, could help confirm the predicted roles of FR-PTC and other cell types in driving fibrosis or repair.
9. Lack of Focus on Potential Therapeutic Implications: The identification of unique cellular niches and interactions presents an opportunity to discuss potential therapeutic targets, especially in the context of failed-repair cells and their associated signaling pathways. Including a discussion on how these insights could inform treatment strategies would enhance the clinical relevance of the study.
10. Integration with Existing Studies: The discussion could benefit from a deeper integration with recent literature on kidney repair and fibrosis, particularly comparing findings from other spatial transcriptomic studies.

(Remarks on code availability)

Reviewer #3

(Remarks to the Author)
In this study, the investigators have developed a multimodal spatial transcriptomics approach by integrating high-resolution Xenium and whole transcriptome Visium platforms to inspect the molecular and cellular events during injury and repair phases in a mouse model of IRI. Distinct neighborhood cell clusters are identified and the cellular interactions are assessed in neighboring cells. The study introduces a valuable pipeline that can be applied to other settings. However, the following points may assist the authors to improve their work:
1. The study is mainly focused on developing a novel spatial transcriptomics pipeline. Although it is interesting from a technique-development perspective, this work hardly provides novel insights about the underlying events during AKI. Indeed, most of the findings of this study on the molecular pathogenesis of kidney injury are already described in previous works. This could be due to limiting the assessments on special parts of data. For instance, although eight neighborhood clusters are identified, the down-stream analyses are restricted to clusters 4 (injured) and 7 (fibrotic), ignoring interactions in other clusters. This reductionist approach is also evident in other sections. For instance, cell interactions are investigated only in particular time points. An overemphasis on specific cell types and pathways might obscure other important contributors to the disease process, potentially limiting the overall understanding of AKI.
2. The primary limitation of the exploited Xenium platform is its restriction to a panel of only 300 selected genes, which may not adequately capture the full transcriptome landscape necessary for a comprehensive analysis. This constraint could result in a major bias in the downstream analyses, particularly if key markers fall outside the selected gene panel. For

instance, the insufficient mitochondrial markers in the Xenium panel may result in ignorance of a key component in the AKI pathogenesis. Additionally, the single-nucleus RNA sequencing (snRNA-seq) mentioned in the manuscript, neglects mitochondrial transcripts, which can constitute up to 50% of the total cellular transcriptome in kidney cells. Integrating the Xenium and Visium data and performing the downstream analysis based on the whole transcriptome data from Visium, not only the 300 gene set, can compensate this drawback.
3. No data regarding the validation of the animal model is provided. The biochemical and histopathologic assessments provide evidence on the robustness and validity of the model. If such investigations are performed at different time points, they would provide additional advantages in demonstrating the trajectory of injury and repair processes over time.
4. Although the study design is inherently longitudinal, time-course investigations are not comprehensively performed. Time-course analyses of gene expressions and cellular interactions can provide valuable insights on the dynamism of the system. This trajectory analysis is crucial for understanding the dynamic progression of cellular states over time, particularly in the context of AKI and its transition to chronic kidney disease (CKD).
5. The interactions of fibroblasts with other cell types are extensively discussed in this work. However, this cell type is vaguely defined in the literature and other cell types can be mislabeled as fibroblasts. What markers were used to label this cell type? How can they be distinguished from pericytes? In figure 2D, PAS images and spatial transcriptomics data are overlaid to validate cell type annotation but this image does not include fibroblasts. Demonstrating these cells in the PAS images provides a clear evidence about their histologic identity.
6. Although the study presents extensive data on gene expression, there is limited functional validation of the findings. Experimental confirmation of the roles of identified processes would strengthen the conclusions.
7. Minor points: a) in some cases the figures are not cited in the text in appropriate order. For instance Figure 2D is cited before 2A and so on. Additionally, some parts of the figures are not cited. b) The second paragraph of Results: Please provide SD or SE for the correlation indices. c) In line 96, referring to a correlation coefficient of r = 0.66 as a “high” correlation may be misleading. This is equal to an r^2 of 0.44 and a more accurate description would classify this correlation as moderate.

(Remarks on code availability)

Reviewer #4

(Remarks to the Author)
This study by Xuanyuan et al. from Humphreys lab investigates the progression from acute kidney injury (AKI) to chronic kidney disease (CKD) in mouse, emphasizing changes in cellular composition and molecular interactions within the kidney. The Humphreys lab is a pioneering group in the field of single-cell and single-nucleus RNA sequencing (sc/snRNA-seq) and spatial transcriptomics of the kidney.
In this study they used advanced spatial transcriptomics platforms—Xenium for high-resolution single-cell data and Visium for whole transcriptome analysis—the authors examined over one million cells from 12 mouse kidneys across six stages of injury and repair. They identified 20 major kidney cell populations and mapped out distinct cellular neighborhoods. By analyzing ligand-receptor interactions, they revealed critical pathways involved in failed repair, chronic inflammation, and fibrosis, particularly in proximal tubule cells, fibroblasts, and immune cells.
The integration of Xenium and Visium data is a standout feature of the study and represents a pioneering effort in kidney research, marking the first time these two technologies have been used side by side to elucidate the progression from AKI to CKD.
The paper is well-written and easy to follow.
Overall, my comments and suggestions are as follows:

Major comments:
-Please provide the creatinine values as a plot, similar to the BUN data, at different time points in Figure 1.
-Please include the fibrosis score and tubular atrophy assessment, as determined by a pathologist, at different time points in Figure 1.
-Please explain how to choose the 300 genes for the panel for Xentium? Did you use your previous snRNA-seq dataset as reference to choose? Expand on the validation of the 300-gene panel—were any additional pilot studies done to ensure it covered all cell types and relevant disease states?
-Please explain why Baysor was specifically chosen for segmentation. It would be helpful to provide a comparison between Baysor, Cellpose, Stardist, and Deepcell, demonstrating why Baysor is the most suitable method for your dataset.
- It appears that macula densa cells were not clearly identified in the Xenium data, as the prediction score for these cells (SF 1G) is low. You included Pappa2 as a marker for macula densa in the panel. Could there be an issue with the probe? Could you please explain the potential reason for this low identification score?
- Please provide an integration of the Xenium and snRNA-seq datasets. Currently, the study presents a heatmap of the prediction scores, but it would be beneficial to integrate the snRNA-seq and Xenium spatial data and present it as a UMAP, showing marker genes in the integrated dataset. This integrated dataset would offer more comprehensive insights and be highly useful for the study.
- It would be helpful to rename the CNs 1-9 with specific names based on the predominant cell types forming them, such as renaming CN1 as "glomerular niche," etc. This would make it easier to follow and understand the context of each neighborhood.
- Similar to the CNs, the clusters in Figure 5 obtained from Visium could be renamed based on the predominant cell types contributing to their formation, rather than using numbers. This would enhance clarity and make the clusters easier to interpret.

-The text mentions that Visium clusters were manually adjusted to match the spatial organization of CNs identified in Xenium data. Providing more details on how this manual adjustment was performed would improve transparency. Were certain criteria or algorithms used for this process, and how were the adjustments validated to ensure accuracy?
- I believe it would be beneficial to perform a cell colocalization analysis, using a package such as CellTrek, on the clusters/CNs from the Visium data, as well as on the Xenium data. For example, I am particularly interested in seeing the neighboring cells of CN4. This analysis would provide a better understanding of regional cell density and population dynamics in the mouse kidney.
- One of the most interesting aspects of the study is the identification of “inj-PT” and “FR-PT” cells. These seem similar to the populations identified by the Susztak lab (PMID 39048792) as “iPT_VCAM1+” and “iPT_HAVCR1.” The question is whether the cells identified in the present study are indeed analogous to those previously described in humans, as mentioned. A side-by-side comparison would be useful in clarifying this. Additionally, is the “inj-PT” population more associated with disease or inflammatory status? Do “inj-PT” and “FR-PTC” cells interact with each other, and does “inj-PT” potentially develop from “FR-PTC”? This could be explored further through colocalization analysis, which could help answer these questions. Moreover, a trajectory analysis, particularly at the spatial level, would provide valuable insights into the progression and relationship between these cell types.
- The comparison of different deconvolution methods was excellent and much needed. Thank you for including that analysis.
- Does the pseudo-Visium data allow for a more accurate comparison of Xenium and Visium, or is it primarily a validation tool? More explanation on its purpose would strengthen the reader's understanding of this method.
-Please consider expanding the description of BANKSY’s spatial clustering process, as readers unfamiliar with this method might benefit from more details.
-Pathway analysis might benefit from integrating additional tools like IPA (Ingenuity Pathway Analysis) to explore upstream regulators or causal networks.
-The description of image registration between Visium and Xenium data could benefit from more clarity. Consider adding more detail on how manual landmark selection was performed to ensure reproducibility.
- While the focus is on IRI-induced kidney injury, a brief comparison of the molecular characteristics of the CN7 (Cluster 7) with those observed in other models of kidney disease (e.g., diabetic nephropathy) could provide additional context. Are these CNs specific to IRI, or might they be found in other kidney injury models? Such a discussion could broaden the relevance of the findings.
- While the study provides strong evidence for ligand-receptor interactions at the transcriptional level, these findings have not been validated at the protein level. It is crucial to confirm that the upregulated LRIs are functionally active in the tissue microenvironment. They should validate the identified LRIs through immunohistochemistry (IHC) or immunofluorescence (IF) staining at least for some of them such as IL34, Csf1r, etc. This would help confirm the spatial localization and interaction of proteins such as TGF-β, PDGF, IL34 and WNT ligands in the tissue, thereby providing stronger evidence for their role in fibrosis and inflammation.

Minor comments:
-Fig. 2A: Please add color labels for each cell type in the figure.
-Please present a UMAP grouped by samples, along with a plot showing the distribution of each sample within each cell type.
-Please include PEC in Supplementary Figure 2.
- Line 535: There is no Figure S9C in the manuscript. Did you mean Figure S1G?

(Remarks on code availability)
The code was reviewed, and STIM provided clear instructions for installation and usage.
The code for generating the figures and conducting the overall analysis was also checked and found to be comprehensive.

Reviewer #5

(Remarks to the Author)
I co-reviewed this manuscript with one of the reviewers who provided the listed reports. This is part of the Nature Communications initiative to facilitate training in peer review and to provide appropriate recognition for Early Career Researchers who co-review manuscripts.

(Remarks on code availability)

Version 1:

Reviewer comments:

Reviewer #1

(Remarks to the Author)
The authors made great efforts to address my concerns, which I appreciate, but I still have some questions.

1) We have demonstrated a high correlation between our imputed gene expression patterns and the detected gene expression using the genes shared between the Xenium and snRNA-seq data (Response Figure 1A, Supplementary Fig. 10A).

The shared genes are the ones used for imputation. Therefore, the imputed and actual expressions are expected to present high correlation. I would suggest the authors ran some bootstrapping, excluding a percentage of genes from the imputation algorithm and testing the correlation on that subset. A possible study would be the minimum percentage of tissue-specific genes necessary to obtain a satisfactory correlation. This could be a very useful result for future researchers when designing their panel. It would be possible to estimate the adequate proportion of cell marker genes and other genes of interest for a particular study.

2) I appreciate the effort in explaining the spatial localization of specific markers. I want to emphasize that I believe receptor-ligand analysis is one of the technical frontiers of spatial technologies and is poised to provide unique insight into injury mechanisms and potential therapeutic targets. I appreciate the authors pushing the envelope in this particular front. But for that very reason, a precise description of the method and its limitations is essential. The list I provided was not extensive. I suggest the authors provide a supplemental table with the location of these markers in the spatial technologies. Also, and appropriate evaluation of the imputation mechanism would bring confidence into this important result.

3) The authors made a fantastic effort on the code availability. Detailed code is fundamental for science reproducibility, and the authors took a leap in the right direction. There are still a few steps missing in the analysis; for instance, the preprocessing of the file Xenium_all.h5ad is not clearly identified, and there is no script for the package commot. I apologize to the authors if I come across as nit-picky. This package is relevant because its default distance in visium is 500 microns, and therefore, contact interactions have to be evaluated critically, especially in a tissue such as a mouse kidney with very small structures. I want to be clear that the authors are ahead of the curve in code availability, and while more details would be desirable, the repository is at a stage where the effort is yielding diminishing results. Thank you for your effort in making the code available.

(Remarks on code availability)
I believe the repository is a good resource as currently presented.

Reviewer #2

(Remarks to the Author)
I want to thank the authors for their answers and improvements to the manuscript. I have no further comments.

(Remarks on code availability)

Reviewer #3

(Remarks to the Author)
The authors have fully addressed my questions and I do not have additional concerns.

(Remarks on code availability)

Reviewer #4

(Remarks to the Author)
The authors have made substantial improvements in the revised manuscript in response to reviewer comments. I appreciate the extensive efforts they have undertaken, including clarifying methodological choices, incorporating additional validation experiments, and strengthening integration with previous literature. Several of my concerns have been adequately addressed; however, there are still areas that could be further refined to enhance clarity, rigor, and overall impact.
My comments are as follows:
-It would be beneficial to validate the identified neighborhoods using an alternative method such as CellCharter (PMID: 38066188). While the authors have used a cell-based approach for neighborhood identification, incorporating an embedding-based method for validation would help assess whether alternative approaches identify any biologically relevant structures that may have been missed by the current method.
-The identified transcription factors (TFs) require validation at the protein level. For instance, the claim that Runx2 and Spi1 are key transcriptional regulators driving fibrosis is based purely on inferred TF activity scores. Without further validation, these conclusions remain speculative. Please perform IHC or IF to validate the expression and spatial localization of these TFs and their roles in fibrosis.
-Please label the neighborhood names in the heatmaps of Figure 6 and Supplementary Figure 9 to improve interpretability.
-Please include P-values in sections comparing cell-type frequencies, particularly in “Spatial transcriptomics accurately recovers cell type composition dynamics in IRI mouse kidney”, where different cell-type compositions are compared across time points. Adding statistical significance will strengthen the validity of these comparisons.

(Remarks on code availability)
The code for generating the figures and conducting the overall analysis was reviewed and found to be clear and comprehensive.

Reviewer #5

(Remarks to the Author)
I co-reviewed this manuscript with one of the reviewers who provided the listed reports. This is part of the Nature Communications initiative to facilitate training in peer review and to provide appropriate recognition for Early Career Researchers who co-review manuscripts.

(Remarks on code availability)

Version 2:

Reviewer comments:

Reviewer #1

(Remarks to the Author)
I appreciate the effort and thoughtfulness in addressing my questions. I am also very satisfied with the code and data availability. I have no further concerns, and commend Xuanyuan et al. on the great manuscript.

(Remarks on code availability)
Excellent code availability

Reviewer #4

(Remarks to the Author)
The authors have responded thoroughly and effectively to my previous comments. I appreciate the additional analyses and validations provided. All of my concerns have been adequately addressed, and I am satisfied with the revisions.

(Remarks on code availability)
The code used for figure generation and overall analysis was reviewed and deemed well-organized and thorough.

Reviewer #5

(Remarks to the Author)
I co-reviewed this manuscript with one of the reviewers who provided the listed reports. This is part of the Nature Communications initiative to facilitate training in peer review and to provide appropriate recognition for Early Career Researchers who co-review manuscripts.

(Remarks on code availability)

REVIEWER COMMENTS

Reviewer #1 (Remarks to the Author):

In this manuscript Xuanyuan et al. present a dataset of Visium and Xenium spatial transcriptomics along the timeline of progression of IRI. The authors present an interesting analysis of the combined data through registration of the sequential sections. The authors make a commendable job of making the data available, including a platform in the lab webpage that allows interactive exploration of the combined dataset. As the authors clearly stated, such a dataset is of fundamental importance to evaluate computational methods such as cell type deconvolution, which is particularly challenging in an organ such as the kidney.

Thank you for these positive comments.

I believe the codes could be more comprehensive regarding the analysis performed in the interest of reproducibility. For instance, there is no script guiding the reader on how to perform the expression imputation. Several scripts on zenodo to generate figures require the analyzed object. There is a github page presenting some of the analysis, but more scripts for this particular manuscript could be made available.

Response: We thank for your suggestions to include more comprehensive scripts covering all aspects of our analysis. We apologize for omission of the preprocessing scripts. We also recognize that the organization of our reproducible codes make it hard to find the specific script for analysis without description. The imputation step is in folder Supplementary/S9/S9C.ipynb on Zenodo. Additionally, due to the extensive number of figures generated during the revision process, we have moved the reproducible code to GitHub (https://github.com/TheHumphreysLab/IRI_Xenium_Visium) with detailed descriptions and better accessibility.

A xenium dataset with cellular resolution and spatial localization has the potential to be a unique tool to investigate cell cell communication. However, I believe this could significantly be improved on this manuscript. Particularly the results presented on figure 6A. As stated on the main text the authors "integrated reference snRNA-seq data to infer spatially resolved cell-cell communications". This could be rewritten to make clear the expression is imputated for this analysis. It is present on the methods, but it is important enough to warrant a place on the main manuscript. Particularly because some of the communication presented is contradicted by the spatial data generated in this work. For instance, Sema3c is not present on Xenium, while in visium is found on the urothelium;
Nrg1 is found on FR_PT on xenium, but its ligand only in urothelium in visium; the receptor Bmpr2 is present in endothelial cells on the xenium dataset; Csf1 is not found in FR_PT in xenium nor viusim; among other examples.

Response: We appreciated your detailed feedback on this point. We have revised the main text to explicitly state that expression imputation was used in our analysis.

Building on our initial observations of the temporal dynamics of cell-type interaction patterns, we integrated reference snRNA-seq data to infer spatially resolved molecular interaction dynamics across IRI time course. We first impute the missing LR genes in Xenium data based on matched time-point snRNA-seq data (Supplementary Fig. 10 A-B). We then identified cell pairs that were physically close to one another and evaluated the ligand-receptor interaction (LRI) significance using statistical tests (Methods).

You point out several instances where the predicted ligand-receptor interactions from our imputed data seem to contradict the actual spatial expression data from our Xenium and Visium datasets. We appreciate your attention to this and provide clarifications below:

1. We have demonstrated a high correlation between our imputed gene expression patterns and the detected gene expression using the genes shared between the Xenium and snRNA-seq data (**Response Figure 1A, Supplementary Fig. 10A**). This strong correlation increases our confidence in the performance of our imputation method. By combining this accurate imputation with the spatial information in the Xenium dataset, we can generate more authentic ligand-receptor interactions compared to traditional inference methods that rely on single-cell datasets without spatial information.

2. For the specific discrepancies between Xenium and Visium dataset:

- Sema3C and Nrg1 in Visium:
Both Sema3c and Nrg1 ligands are found to be expressed in FR-PT cells in our snRNA-seq data and are reflected in the imputed Xenium data (**Response Figure 1B**). The apparent expression of these genes in the urothelium within the Visium dataset is likely due to the lower spatial resolution of the Visium platform and the method used for spot annotation. In the Visium data, each spot is about 55 μm in diameter, encompassing multiple cell types. We annotated Visium spots based on the highest frequency of Xenium cell types mapped within each spot. This approach can lead to misannotation when multiple cell types are present within a single spot. When overlaying the Visium gene expression of Sema3c and Nrg1 with the Xenium cell labels, we found that Visium spots with strong expression of Sema3c and Nrg1 correspond spatially to regions rich in FR-PT cells, not urothelial cells (**Response Figure 2**).

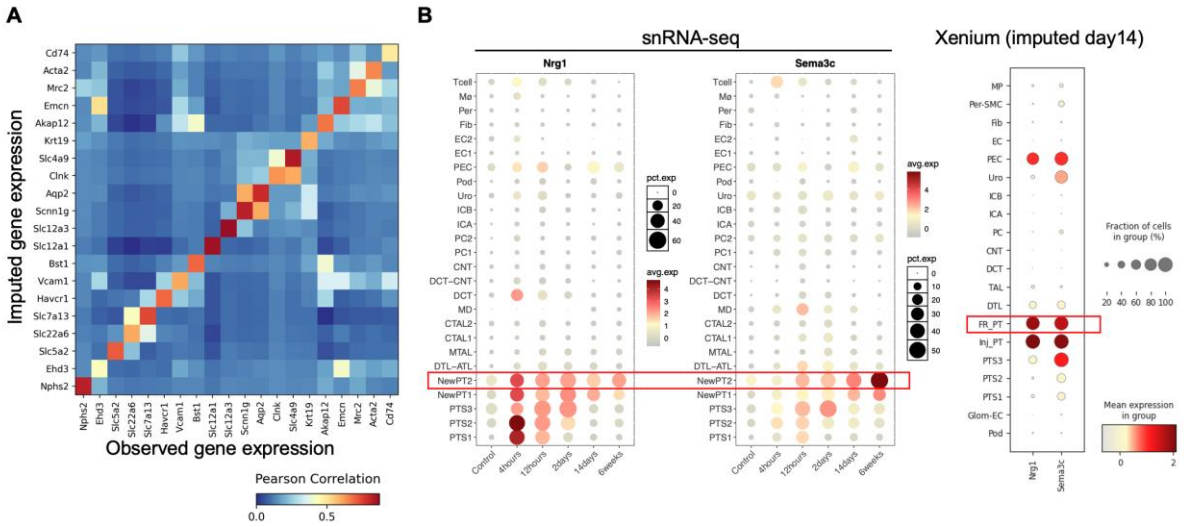

Response Figure 1. **A.** Correlation between observed expression and imputed expression. **B.** Dot plot showing the expression levels of Nrg1 and Sema3c in snRNA-seq data and Xenium data at day 14.

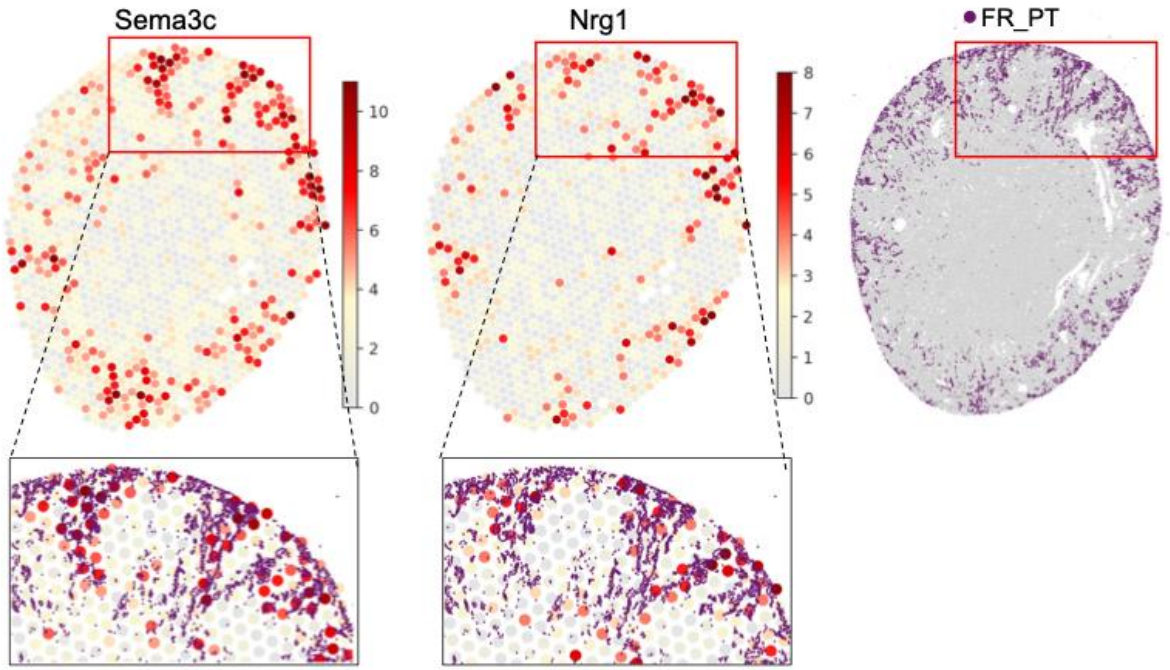

Response Figure 2. Spatial gene expression patterns of Sema3c and Nrg1 in the Visium day 14 sample. Raw counts with a 0.99 quantile max cutoff were used for visualization. The overlay of gene expression on FR-PT cell spatial distribution indicates a high correspondence between the expression of these genes and the location of FR-PT cells.

- Bmpr2 expression and Csf1 expression:
We acknowledge that Bmpr2 is predominantly expressed in endothelial cells; however, our data indicate that some fibroblasts also express Bmpr2 in both our spatial datasets and the snRNA-seq data. In the spatial data from day 14 post-IRI, we observed that the transcript distribution of the Bmp6-Bmpr2 ligand-receptor pair shows co-localization patterns consistent with interactions between FR-PT cells and fibroblasts. Similarly, for Csf1, we have identified its expression in FR-PT cells in the Xenium dataset. The co-localization of Csf1 and Vcam1 transcripts supports the presence of Csf1 in FR-PT cells. The Csf1-Csf1r co-localization patterns consistent with interactions between FR-PT cells and immune cells (**Response Figure 3**).

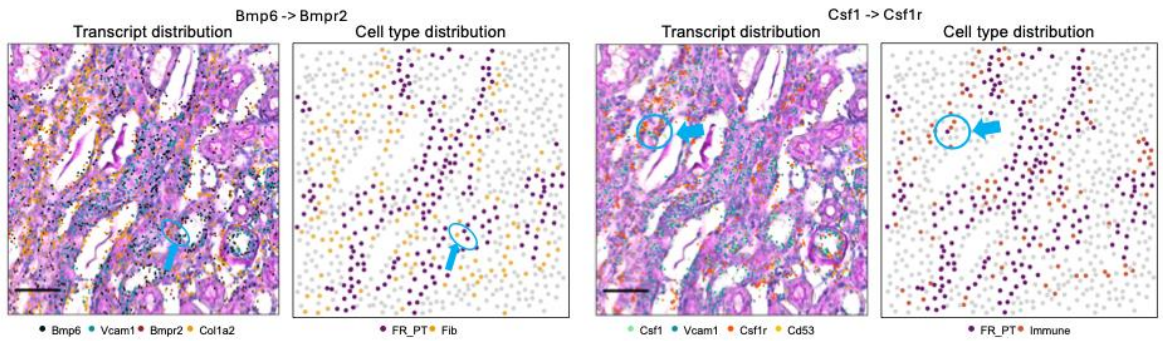

Response Figure 3. Spatial transcript distribution showing the co-localization of ligand-receptor pairs Bmp6-Bmpr2 and Csf1-Csf1r in the day 14 post-IRI dataset. Transcripts for Vcam1 (FR-PT cell marker), Bmp6 (ligand), Col1a2 (fibroblast marker), Bmpr2 (receptor), Cd53 (immune cell marker), and Csf1r (receptor) are displayed. The blue arrow highlights an example of a potential cell-cell interaction based on transcript co-localization.

Here is an update of our ligand-receptor analysis according to other reviewers' comments: (1) We have expanded our analysis to include cell-cell and cell-ECM interactions. (2) We have expanded our analysis across all time points post-IRI. The updated results are presented in the **Main Fig. 6.**

Regarding novelty, the authors provide a rich dataset characterizing a model of acute kidney injury. The xenium dataset is of particular value, as it may also guide the panel selection of future studies. I would also like the authors to better contextualize how the findings in this paper characterizing the failed repair proximal tubule, and some of the identified communication, such as Ccl2 or Csf1, add to the previous description of this model by the lab on Muto et al.

Response: We thank the reviewer for this comment. In the study by Muto et al., we used snATAC-seq to identify the key regulators driving the fate commitment of FR-PTCs. In particular, we found the activation of NF-κB signaling in FR-PTC at day 14 post-IRI. However, due to the loss of spatial context inherent to single-nucleus isolation—a necessary step for generating snATAC-seq data—how the dysregulated NF-κB signaling impacts cell-cell interactions remained unclear. In this manuscript, we identified *Nfkb1* as one of the top predicted upstream transcription factors within the

fibrotic niche (**Main Fig. 5G**) and contextualized the ligand-receptor interactions between FR-PTC and immune cells including *Ccl2-Ccr2, Csf1-Csf1r* (**Main Fig. 6A**). We have added related discussion in the revised manuscript.

Overall, I believe this manuscript is well written, and the generated dataset is valuable to the community.

Thank you.

Reviewer #1 (Remarks on code availability):

There is no code that reproduces the results. There is a github page with some similar examples, and the code available in zenodo generates displays based on processed data.

We have moved the reproducible code to GitHub for better accessibility and added detailed descriptions.

Reviewer #2 (Remarks to the Author):

The manuscript "Multimodal Spatial Transcriptomic Characterization of Mouse Kidney Injury and Repair" by Xuanyuan et al. presents a detailed spatial analysis of acute kidney injury (AKI) using bilaterial IRI mouse model, employing two complementary technologies: Xenium and Visium. The study analyzes 12 mouse kidneys across six stages of disease progression, focusing on dynamic changes in spatial cellular neighborhoods that cannot be captured with single-cell RNA sequencing alone. Notably, the study highlights failed-repair proximal tubular cells (FR-PTC), which form unique niches with fibroblasts and immune cells.

While the data quality is high and the findings are insightful, the study could benefit from further exploration of biological insights. Recent spatial datasets, such as Polonsky et al. using SeqFISH+ in Nature Communications, targeted 1,300 genes but analyzed only a single time point (day 28). The distinctiveness of this manuscript lies in its integration with Visium, a full-transcriptome spatial assay from the same section, allowing for a more comprehensive temporal analysis.

However, the manuscript currently mixes data description with benchmarking of spatial software tools, which detracts from the focus on biological insights, which are currently underexplored. A clearer narrative on the biological implications is needed.

Below are key points that require attention:
1. Sample Size and Sex Differences: The sample size of n=2 per time point is too low, particularly for analyzing sex-specific differences. Including tissues from models treated

with antifibrotic drugs (e.g., Finerenone or SGLT2 inhibitors) could provide additional insights.

Response: We acknowledge that sample size for this study is low compared to traditional single-cell studies. Unlike single cell studies where each replicate includes thousands of cells, each sample in our Xenium dataset contains about 100,000 cells. This high cell count per sample provides a rich dataset allows for robust analyses within each biological replicate. Each Xenium experiment involves considerable expense and time, which constrained the number of samples we could include in this study.

We apologize for not explicitly stating in the original manuscript that only male mouse kidneys were used in this study. Our goal was not to investigate sex-based variations. We have revised the title and relevant sections of the manuscript to clearly state that only male mice were used in this study.

We appreciate your valuable suggestion to explore additional mouse models using spatial technologies. However, our current study is primarily focused on characterizing the natural progression of kidney injury and repair without examining the effects of therapeutic interventions. We acknowledge that studying therapeutic effects is an important future direction.

2. Cell Type Composition and Validation: The comparison of cell-type compositions between spatial transcriptomics and single-cell data should be further validated, potentially at the protein level. Deconvolution of the Visium data should confirm observed cell-type changes, yet these findings currently add little to the biological narrative.

Response: We appreciate the suggestion to validate our cell type composition results in Xenium data. We have observed that fibroblasts are underrepresented in snRNA-seq studies compared with *in situ* Xenium spatial transcriptomics due to challenges in cell dissociation. To confirm this observation at the protein level, we performed new Picrosirius Red staining on slides from the same tissue samples used in our study. Please refer to the Method section "**Pathology Score Assessment**" for detailed methodology description on the fibrosis level quantification. Briefly, we quantified the extent of interstitial fibrosis by calculating the percentage of Sirius Red-positive areas over the total kidney tissue area. Our analysis revealed a significant correlation between the fibroblast proportion calculated from the Xenium dataset and the quantified fibrosis score (p-value adjusted using Bonferroni correction) (**Response Figure 4 A-B**). This strong correlation provides good validation of our cell-type composition analysis.

Furthermore, we compared the deconvoluted fibroblast frequencies obtained from the Visium data using different deconvolution algorithms (**Response Figure 4C**). We found that none of the Visium-deconvoluted fibroblast frequencies showed a significant correlation with the fibrosis score. This observation aligns with our benchmarking results, indicating that Visium deconvolution methods may introduce biases and have limitations in accurately reflecting true cell compositions for specific cell types. By

validating the fibroblast abundance through both transcriptomic data and histopathological staining, we highlight the critical role of fibroblasts during the development of fibrosis following AKI.

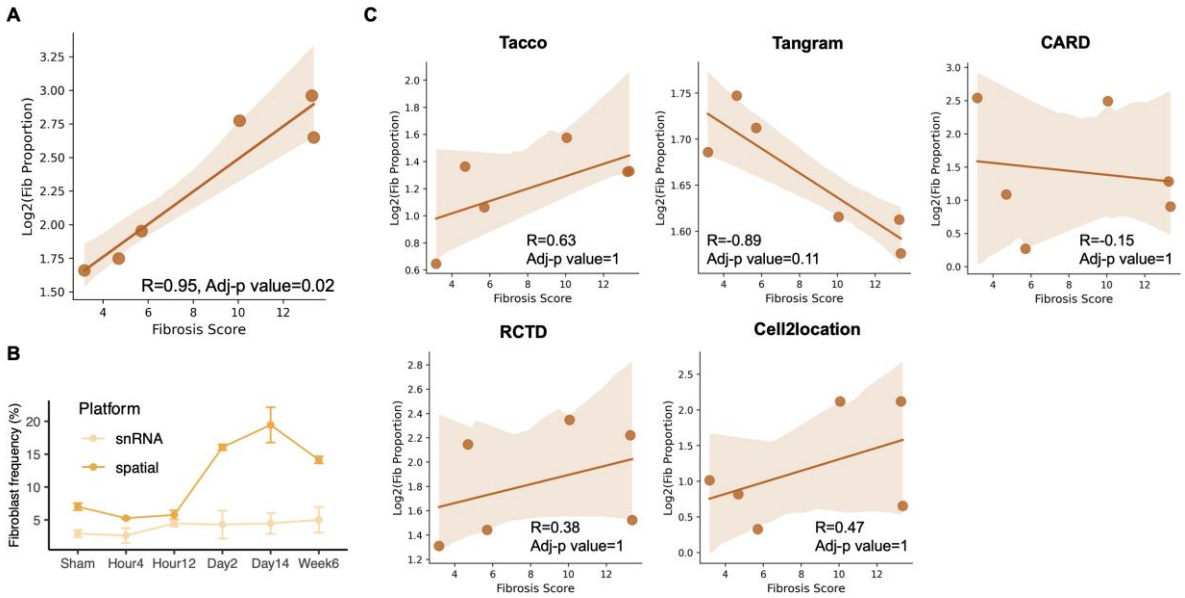

Response Figure 4. **A.** Correlation between fibroblast abundance (log transformed) and the quantified fibrosis score from Sirius Red staining images. **B.** Temporal distribution of fibroblast frequency in snRNA-seq and Xenium spatial dataset. **C.** Correlation between the deconvoluted fibroblast abundance and the fibrosis score across different deconvolution algorithms.

3. Cell Neighborhood Analysis: The rationale for the chosen the described spatial neighborhood approach needs elaboration. Tools like CellCharter or NichePCA could offer a more robust analysis of spatial domains and their temporal dynamics. Clarifying why these specific approaches were chosen over others would strengthen the methodological transparency.

Response: We appreciate your insightful comments regarding our cell neighborhood analysis and the opportunity to clarify our methodological choices.

There are two primary approaches to define cell neighborhoods: one is cell-based method, where neighborhoods are defined based on the composition of cell types within a local area. The other is gene-expression embedding-based method, where neighborhoods are defined based on local gene expression profiles using dimensionality reduced features.

Rationale for choosing current cell-based method:

1. Our xenium dataset offers single-cell resolution but measures expression for only 300 genes. Cell-based methods could effectively capture the organizational features of the

tissue and provide direct interpretability. Embedding-based methods are more susceptible to technical noise in datasets with limited genes.

2. Our goal was to link structural and organizational features identified in Xenium with molecular functions in Visium. To achieve this, we performed Visium whole-transcriptome sequencing on adjacent tissue sections. We deconvoluted Visium spots using the cell-type frequencies derived from Xenium and assigned CN labels to Visium spot based on their local cell composition similarity. We effectively recreated the structural organization identified in Xenium at the Visium resolution. By doing this, we could align structural features with molecular functions.

We conducted a comparative evaluation of our cell-based method with CellCharter[1] and NichePCA[2], focusing on computational efficiency and gene signature similarity.

1. Our dataset comprises about 1.3 million spatial data points. Both CellCharter and NichePCA requires several hours to identify spatial domains, whereas our cell-based method completed this task in approximately 1 minute (**Response Figure 5A**).

2. We compared the cell neighborhoods identified by our method and other methods by analyzing the top 20 contributing genes for each neighborhood. We computed the Jaccard similarity index to quantify the overlap of gene signatures between the methods. For CellCharter, we selected the number of clusters (n=8) based on cluster stability analysis provided by the package (**Response Figure 5B**). However, we observed similar stability across different cluster numbers (n=2 to n=9). This may be due to the limited feature space of 300 genes, which make the clustering algorithm less sensitive to subtle distinctions between neighborhood clusters. The Jaccard index highlight the conserved signatures between most neighborhoods identified in both CellCharter and our method (**Response Figure 5C**). For NichePCA, this method was unable to identify biologically meaningful structures compared to CellCharter or our cell-based method (**Response Figure 5D-E**). We believe this limitation arises from NichePCA's reliance on aggregating gene expression across neighborhoods followed by dimensionality reduction (PCA). Given our dataset's limited gene panel, the PCA embedding lacks sufficient variance to effectively capture and differentiate the complex biological heterogeneity present in the tissue, resulting in reduced performance in identifying distinct and meaningful spatial domains.

In response to the reviewer’s suggestion on the rationale, we have provided a detailed explanation of the choice in the method “**Cell Neighborhood Analysis**” section. We have updated the approach to transfer Xenium neighborhood labels to Visium dataset. This new strategy also requires defining neighborhood based on local cell-type composition instead of gene expression (**Main Fig. 5**).

Reference

1. Varrone, M., Tavernari, D., Santamaria-Martínez, A., Walsh, L. A. & Ciriello, G. CellCharter reveals spatial cell niches associated with tissue remodeling and cell plasticity. *Nat. Genet.* **56**, 74–84 (2024).
2. Schaub, D. P. *et al.* PCA-based spatial domain identification with state-of-the-art performance. *bioRxiv* 2024–07 (2024).

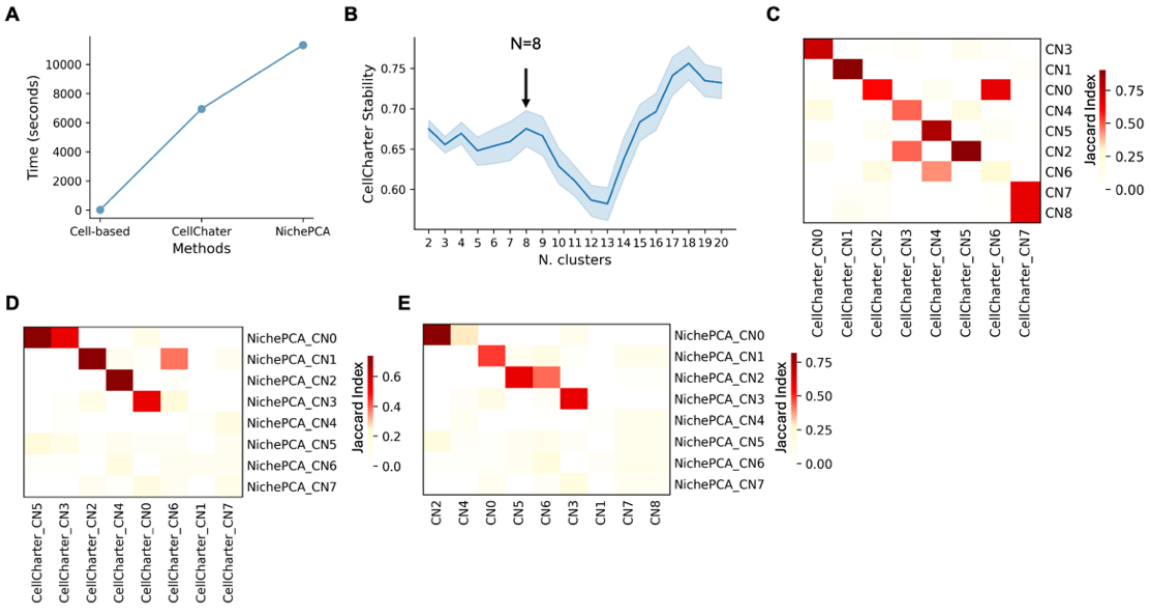

Response Figure 5. **A.** Run time for three methods on our Xenium dataset. **B.** CellCharter cluster stability. **C.** Comparison between cell neighborhoods using our cell-based and CellCharter using the top 20 marker genes in each CN. **D-E.** Comparison between cell neighborhoods using NichePCA with our method and CellCharter using the top 20 marker genes in each CN.

4. Benchmarking Deconvolution Methods: Although the benchmarking of deconvolution tools is informative, it diverts from the manuscript's main biological focus. Integrating deeper biological analysis would strengthen the study. The emphasis on tool performance over biological discovery can distract readers from the core findings.

Response: Thank you for your feedback. We understand your concern that the inclusion of benchmarking deconvolution methods may divert attention from the main biological focus. In response to your suggestion, we have moved the benchmarking section to the **Supplementary Note 2** so that the main text will emphasize on the biological implications of our findings.

However we believe that the benchmarking result is crucial for the following reasons:

1. One of the unique strengths of our study is the multi-modal spatiotemporal profiling of the kidney using adjacent sections, which provides actual ground truth cell type

compositions in Visium spots. Our benchmarking revealed that some deconvolution algorithms tend to overestimate certain cell populations, such as immune cells. This overestimation could lead to misleading conclusions about the extent of inflammation and the state of disease progression. In our study, instead of using deconvolution algorithms, we deconvoluted Visium spots by aggregating Xenium cell on adjacent section. By rigorously validating the deconvolution tools, we not only enhance the reliability of our findings, but also alert the research community to potential pitfalls in data analysis.

2. Our dataset offers a valuable opportunity to benchmark deconvolution tools using real-world ground truth data, rather than relying on simulated datasets. Simulated data may not capture the full complexity and variability of actual biological samples, potentially leading to overestimated performance metrics. By providing an evaluation of these tools in a realistic setting, we provide the research community with critical insights into the practical performance of the algorithms.

5. Spatial Data Integration: The manuscript describes a binning approach to integrate Visium and Xenium data, involving manual adjustments to achieve shared cellular compositions. This method could introduce biases, and alternative approaches should be considered. A quantitative assessment of how this manual integration impacts results would be beneficial.

Response: We appreciate the reviewer's feedback regarding the manual adjustment of Visium clusters to match the spatial organization of cell neighborhoods identified in Xenium data. We acknowledge that manual adjustments can introduce bias and may lack reproducibility. We have utilized an alternative method to assign labels to Visium spots based on their structural organization. We have updated all the downstream analysis results on Visium using this new method. Below is the method detail:

We constructed cell composition matrices for both the Xenium and Visium datasets by matching their spatial scales. For the Xenium data, we calculated local cell type frequencies within a 55-micron radius around each cell, corresponding to the size of a Visium spot. For the Visium data, we deconvoluted each spot to estimate the proportion of each cell type present based on reference Xenium data. We performed PCA on combined matrix to obtain a joint embedding of the two datasets. To match the Visium spot to Xenium cell neighborhood, we identified the top 20 nearest neighbors given a Visium spot based on the joint embedding. We assigned the cell neighborhood label to each Visium spot based on majority voting among the labels of these nearest Xenium cells (**Response Figure 6A, Main Fig. 5C**).

To demonstrate the robustness of our label transfer, we performed a leave-one-out (LOO) cross-validation on the Xenium data. In each iteration, one Xenium cell was left out, and the remaining cells were used for integration with the Visium data to predict the neighborhood label for the left-out Xenium cell. The overall prediction accuracy was 0.84, indicating a high level of confidence in our ability to recreate the structural organization identified in Xenium at the Visium resolution (**Response Figure 6B,**

Supplementary Fig. 14). Gene signature comparison also demonstrates a high level of concordance between the neighborhood clusters in both datasets (**Response Figure 6C, Main Fig. 5D**).

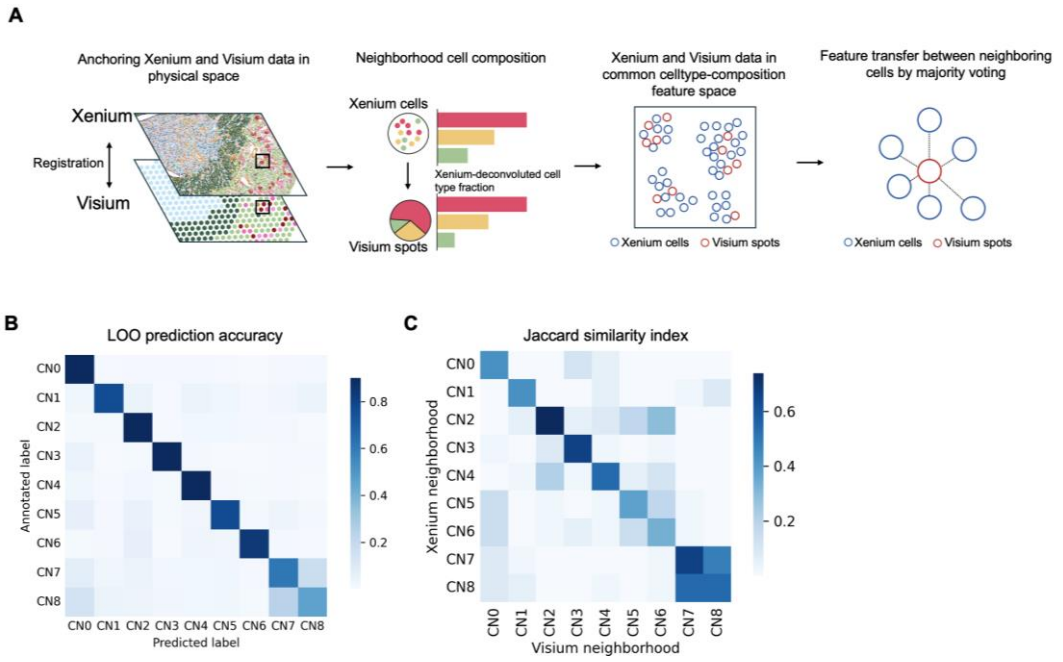

Response Figure 6. **A.** Schematic workflow of Xenium/Visium integration and cell neighborhood label transfer. **B.** Leave-one-out cross-validation performance across cell neighborhood clusters. **C.** Heatmap of Jaccard index of top 20 gene signature similarity between corresponding neighborhood clusters from Xenium and Visium datasets. Higher values indicating greater overlap in gene expression profiles.

6. Receptor-Ligand Interactions: The current analysis using CellChat lacks dynamic exploration of cell-cell communication (CCC). NicheNet could provide a more comprehensive modeling of intercellular communication, especially given the time-course nature of the data. The authors should aim to link CCC findings to specific biological outcomes, such as fibrosis predisposition within certain tissue niches.

Response: We thank the reviewer for commenting on our receptor-ligand analysis. We apologize for any misunderstanding in our method description. While we utilized the CellChat database[1] for ligand-receptor interaction, we did not use the CellChat software tool for our analysis. Instead, we leveraged the spatial information in Xenium dataset to infer potential cell-cell communications. NicheNet[2] is also primarily designed for single-cell RNA-seq data and does not incorporate spatial localization of cells. Given the importance of the spatial context, we chose a method which integrates both gene expression data and spatial information, allowing us to identify significant ligand-receptor interactions based on co-expression and cell proximity.

We use our paired snRNA-seq data to impute the missing genes in our Xenium dataset, thereby expanding the number of ligand-receptor genes included in our analysis. We observed strong correlation between the imputed spatial pattern and the measured spatial pattern for cell type marker genes (**Response Figure 1A**). Using the imputed Xenium dataset, we conducted a spatially based cell-cell interaction analysis inspired by method described by Zhang et al[3]. Our analysis involved three important steps: 1. We defined the proximal sender-receiver cell type pairs which are within a distance of 30 microns of each other. This distance covered both the direct cell-cell contacts and paracrine communication. 2. To assess the significance of observed interactions, we randomly selected cell pairs that were not proximal (cell pairs located more than 30 microns apart) to serve as a null distribution. 3. We performed statistical tests (one-sided t-test) to determine whether the co-expression of ligand-receptor pairs was significantly higher in proximal cell pairs compared to non-proximal pairs (**Methods**).

Previously, our CCC analysis focused primarily on secreted signaling proteins. We have expanded our analysis to include "ECM-receptor" interactions and "cell-cell contact" to capture a broader range of interactions. We have revised **Fig. 6A** to include these additional interactions and have further investigate how these ligand-receptor interactions related to disease progression, specifically fibrosis development within the FR-PT enriched neighborhood.

Reference

1. Jin, S. *et al.* Inference and analysis of cell-cell communication using CellChat. *Nat. Commun.* **12**, 1088 (2021).
2. Browaeys, R., Saelens, W. & Saeys, Y. NicheNet: modeling intercellular communication by linking ligands to target genes. *Nat. Methods* **17**, 159–162 (2020).
3. Zhang, M. *et al.* Molecularly defined and spatially resolved cell atlas of the whole mouse brain. *Nature* **624**, 343–354 (2023).

7. Limited Exploration of Longitudinal Changes: Although the study spans multiple time points, the temporal dynamics of key molecular and cellular interactions are underexplored. Highlighting changes in receptor-ligand interactions or shifts in cell state populations over time would add valuable context to the findings.

Response: Thank you for your insightful comment regarding the limited exploration of longitudinal changes in our study. In response to your feedback, we have conducted two additional time-course analysis to investigate both temporal changes in cell-type interactions and dynamics of molecular interactions (time course LR-analysis).

We performed a proximity-based cell interaction analysis across IRI time course to illustrate how cell type interactions evolve over time. We calculated the interaction frequency between pairs of cell types at each time point using permutation tests. Interaction strengths were assessed using z-scores indicating the magnitude of observed interaction frequency compared with random distributions. We observed

consistent strong interaction between immune cells and fibroblasts across all time points post-injury. At day14 post-injury, FR-PT cells exhibited strong interaction with both immune cells and fibroblasts (**Response Figure 7**). We have included the longitudinal co-localization analysis in the revised manuscript (**Main Fig. 4E and Supplementary Fig. 7**).

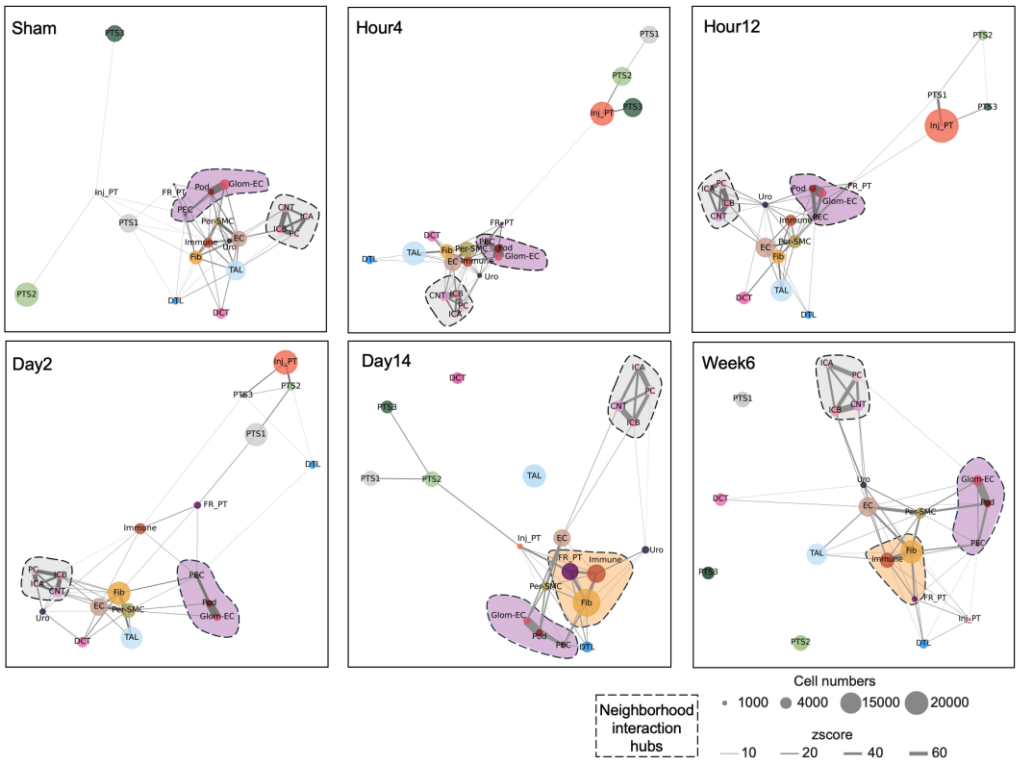

Response Figure 7. Colocalization between cell types across IRI time points. Node size represents the number of cells for each cell type and edge width represents the colocalization z-score.

We have also extended our cell-cell communication analysis across the IRI time course. We conducted a spatially resolved LR analysis using our high-resolution Xenium dataset, as well as on Visium dataset. With imputed Xenium dataset, we identified significant LR pairs (adjusted p-value<0.05, co-expression fraction>0.5, log Fold Change>1) and visualized the top LR interactions in **Main Fig. 6A**. Similarly, we performed time-course cell-cell communication on Visium dataset using COMMOT. We added visualizations of the spatiotemporal dynamics of the signaling activities in **Supplementary Fig. 11.**

8. Biological Validation: The study relies heavily on computational predictions without sufficient experimental validation. Functional assays, such as knockdown or overexpression studies, could help confirm the predicted roles of FR-PTC and other cell types in driving fibrosis or repair.

Response: Thank you for highlighting the need for experimental validation. In this revision, we have added experimental data to validate the cell-cell communication between FR-PTC and other cell types. We performed immunofluorescent staining to confirm the spatial proximity and ligand-receptor interactions between FR-PTC and immune cells mediated by ICAM1-ITGB2.

Besides the immunostaining, both the Xenium and Visium datasets cross-validate our computational predictions, thereby enhancing the confidence in our findings.

We have added this validation data to the result section as below:

Our LRI analysis suggests that direct contact between FR-PT cells and immune cells is mediated by adhesion molecules and integrins including intercellular adhesion molecule 1 (ICAM1) and β2-integrin (ITGβ2). This caught out attention because β1-integrin was recently shown to mediate interactions between medullary macrophage and the tubular epithelium when forming transepithelial protrusion that help remove intratubular debris[1]. Immunostaining revealed co-localization of ICAM1 on VCAM1+ FR-PT cells and ITGB2 on F4/80+ macrophages. Orthogonal imaging of a longitudinally sectioned VCAM1+ tubule shows abluminal F4/80+ macrophage (yellow arrowheads) with ITGB2+ extensions (see white arrowheads in zy and zx planes) extending across the epithelial membrane.

Reference

1. He, J. *et al.* Renal macrophages monitor and remove particles from urine to prevent tubule obstruction. *Immunity* **57**, 106-123.e7 (2024).

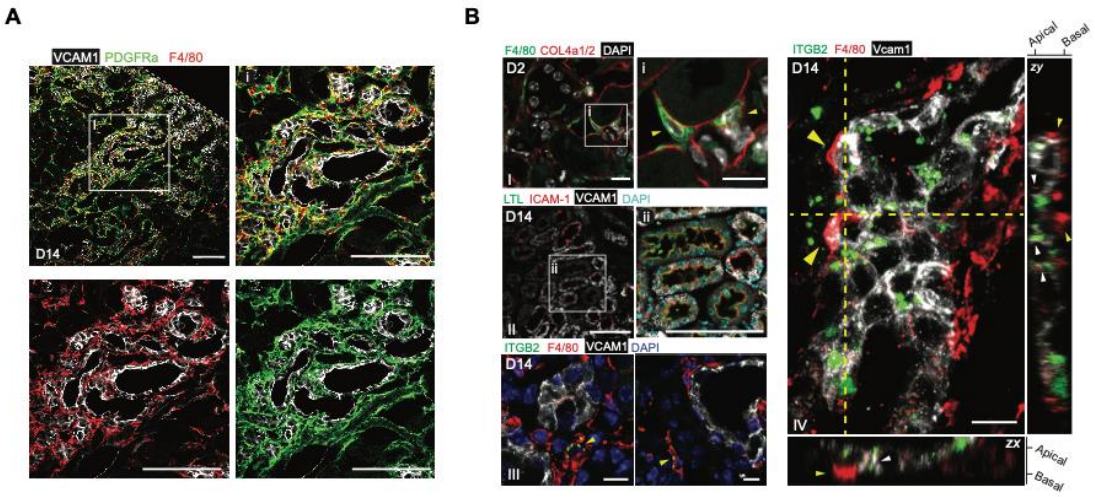

Response Figure 8. **A.** Immunofluorescent staining indicates the spatial proximity between VCAM1+ FR-PT cells, F4/80+ macrophages and PDGFRα+ fibroblasts. Scale bar = 100 μm. **B.** Immunofluorescent staining of ICAM1 and ITGβ2. I. F4/80+ macrophages within peritubular space on abluminal side of tubular basement membrane marked by COL4α1/2. II. ICAM1 expression in VCAM1+ LTL tubules after bilateral IRI. III. ITGβ2+F4/80+ macrophage neighbour VCAM1+ tubules in injured kidneys. IV. Orthogonal views of a longitudinally sectioned VCAM1+ tubule and two ITGβ2+F4/80+ macrophage. Yellow arrowhead denotes a macrophage. White arrowheads denote macrophage extensions. Scale bar = 10 μm (I, II, III) and 100 μm (IV).

9. Lack of Focus on Potential Therapeutic Implications: The identification of unique cellular niches and interactions presents an opportunity to discuss potential therapeutic targets, especially in the context of failed-repair cells and their associated signaling pathways. Including a discussion on how these insights could inform treatment strategies would enhance the clinical relevance of the study.

Response: Thank you for the suggestion of adding clinical relevance of the study. In the revised manuscript, we have incorporated additional text in the Discussion section to emphasize the clinical relevance of the study (line 2008-2083).

10. Integration with Existing Studies: The discussion could benefit from a deeper integration with recent literature on kidney repair and fibrosis, particularly comparing findings from other spatial transcriptomic studies.

Response: Thanks for your suggestion. In the revised manuscript, we have expanded our comparison of the gene signature identified in the fibro-inflammatory niche (CN7) with data from Polonsky (2024) (mouse IRI) and Abedini (2024) (human CKD) (**Response Figure 9, Supplementary Fig. 9E, F).** We quantified the average expression levels of neighborhood-derived DE genes across cell types identified in mouse IRI and human CKD datasets. We observed a consistent enrichment of CN7

activity in similar cell populations, particularly injured PT cells and fibroblasts. In both datasets, disease samples (e.g., 28-day post-IRI kidneys in mice and CKD kidneys in humans) demonstrated significantly elevated CN7 activity compared to controls.

Based on these findings, we added additional text in the Discussion section (line 1987-1995).

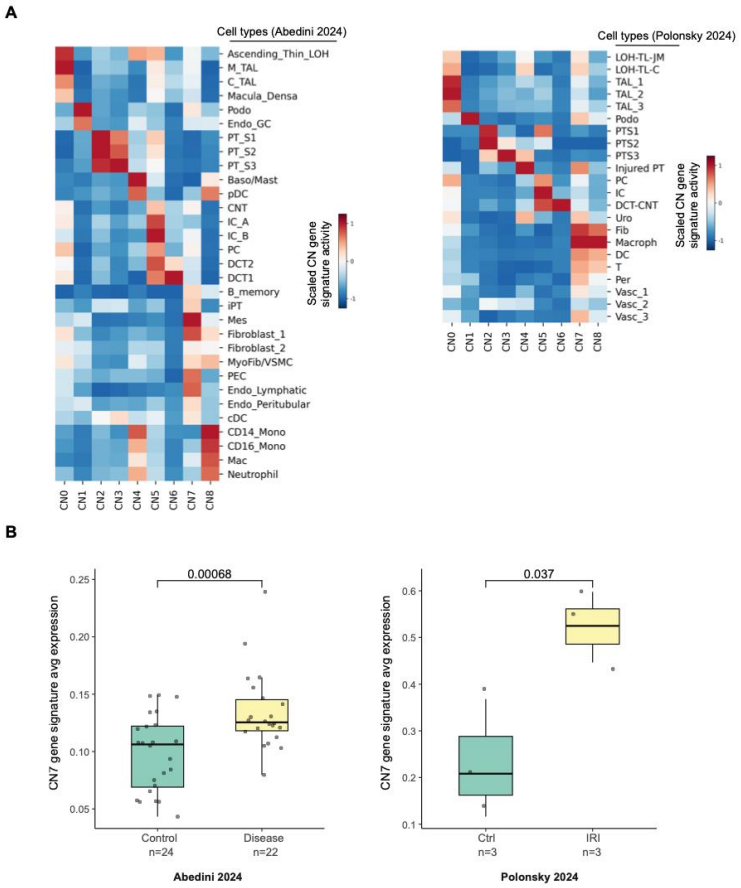

Response Figure 9. **A.** Heatmap highlighting the activity of gene signatures derived from each cell neighborhood across cell types in the Abedini (human) and Polonsky (mouse) spatial datasets. B. Boxplot comparing the distribution of fibro-inflammatory niche (CN7) derived gene signatures between healthy and diseased kidney samples in mouse and human datasets.

Reviewer #3 (Remarks to the Author):

In this study, the investigators have developed a multimodal spatial transcriptomics approach by integrating high-resolution Xenium and whole transcriptome Visium platforms to inspect the molecular and cellular events during injury and repair phases in a mouse model of IRI. Distinct neighborhood cell clusters are identified and the cellular

interactions are assessed in neighboring cells. The study introduces a valuable pipeline that can be applied to other settings. However, the following points may assist the authors to improve their work:

1. The study is mainly focused on developing a novel spatial transcriptomics pipeline. Although it is interesting from a technique-development perspective, this work hardly provides novel insights about the underlying events during AKI. Indeed, most of the findings of this study on the molecular pathogenesis of kidney injury are already described in previous works. This could be due to limiting the assessments on special parts of data. For instance, although eight neighborhood clusters are identified, the down-stream analyses are restricted to clusters 4 (injured) and 7 (fibrotic), ignoring interactions in other clusters. This reductionist approach is also evident in other sections. For instance, cell interactions are investigated only in particular time points. An overemphasis on specific cell types and pathways might obscure other important contributors to the disease process, potentially limiting the overall understanding of AKI.

Response: Thank you for raising this important concern. In our study, we chose to focus on CN4 and CN7 because they represent two critical injured proximal tubule cell niches within distinct phases of injury: the early Havcr1+ tubule for CN4 and late Vcam1+ tubule for CN7. Building upon our previous work and that of others, we focused on these neighborhoods to investigate how specific cell-cell interactions may drive the transition from AKI to CKD.

We acknowledge that other neighborhoods also play important roles in AKI pathogenesis. Our targeted approach allows for a more cohesive investigation of how FR-PTCs interact with immune cells and fibroblasts during fibrosis progression. To ensure that other researchers can explore additional questions using our datasets, we have provided a computational toolkit to explore our spatial dataset and a static visualization tool publicly available (https://humphreyslab.com/SingleCell/search.php).

To address the concern of only a single time point was investigated, we have expanded our analysis to encompass all time points on both cell-type interactions and molecular interactions. Please refer to **Reviewer 2 questions 6–7** for the longitudinal analysis**.**

2. The primary limitation of the exploited Xenium platform is its restriction to a panel of only 300 selected genes, which may not adequately capture the full transcriptome landscape necessary for a comprehensive analysis. This constraint could result in a major bias in the downstream analyses, particularly if key markers fall outside the selected gene panel. For instance, the insufficient mitochondrial markers in the Xenium panel may result in ignorance of a key component in the AKI pathogenesis. Additionally, the single-nucleus RNA sequencing (snRNA-seq) mentioned in the manuscript, neglects mitochondrial transcripts, which can constitute up to 50% of the total cellular transcriptome in kidney cells. Integrating the Xenium and Visium data and performing the downstream analysis based on the whole transcriptome data from Visium, not only the 300 gene set, can compensate this drawback.

Response: We appreciate the reviewer's comment on the limitation of this study. Spatial transcriptomics techniques inevitably present trade-offs between the resolution, sensitivity and gene coverage. We acknowledge the limitation of gene panel in our Xenium dataset and have employed several approaches to address it.

First, we integrated the Xenium dataset with our previously published snRNA-seq dataset generated from the same bIRI mouse models. Through reference mapping, we confirmed the accuracy of our cell type annotations in the Xenium data compared with the predicted labels from snRNA-seq data (**Supplementary Fig. 1H, I**). We also added a new supplementary figure (**Supplementary Fig. 3**) depicting the co-embedding of the Xenium and snRNA-seq dataset on a shared UMAP feature space. Additionally, we applied computational approach including gene imputation to expand the Xenium panel, which allow us to investigate the missing genes during the ligand-receptor analysis.

Second, we performed Visium on adjacent tissue sections to Visium which has genome-deep coverage but limited in spatial resolution. This joint analysis of Visium and Xenium datasets helps mitigate the limitations associated with the Xenium platform. After transferring the neighborhood labels from Xenium to Visum data, we were able to functionally characterize the identified neighborhoods in more detail.

We acknowledge that these approaches were not specifically designed to study the mitochondrial aspects of PT cells, but this is not the focus of the current manuscript. We have previously published multiomics datasets which we believe serve as more valuable resource for studying mitochondrial related pathways of the tubular cells in IRI[1,2].

In the discussion section, we have addressed the limitations of current study and proposed future directions based on our findings.

Reference:
1. Yoshiharu Muto et al. ,Epigenetic reprogramming driving successful and failed repair in acute kidney injury.Sci. Adv.10,eado2849(2024).DOI:10.1126/sciadv.ado2849
2. Y. Kirita, H. Wu, K. Uchimura, P.C. Wilson, B.D. Humphreys, Cell profiling of mouse acute kidney injury reveals conserved cellular responses to injury, Proc. Natl. Acad. Sci. U.S.A.117 (27) 15874-15883, https://doi.org/10.1073/pnas.2005477117 (2020).

3. No data regarding the validation of the animal model is provided. The biochemical and histopathologic assessments provide evidence on the robustness and validity of the model. If such investigations are performed at different time points, they would provide additional advantages in demonstrating the trajectory of injury and repair processes over time.

Response: Thank you for your suggestion regarding the validation of the animal model. We have performed two histopathologic assessments: 1) Quantification of tubular lesion score on PAS-stained images. 2) Quantification of fibrosis score on Sirius red-stained

images. We have added a detailed description of the quantification workflow to the Methods section of the manuscript.

In the tubular lesion score assessment, we observed a gradually increase in the tubule-interstitial lesion score post-injury (**Response Figure 10A-B**). Although there was a decrease in the injury score after day2, it did not return to baseline levels by week 6, indicating incomplete tubular repair after IRI. For the fibrosis score, we found a sustained increase in the interstitial fibrosis level starting at day2 post-injury (**Response Figure 10C-D**). The fibrosis score remained high until week6, confirming the development of fibrosis following AKI. Both the tubular lesion injury score and fibrosis score validate the use of our animal model to study the spatiotemporal dynamics of AKI and progression to CKD.

Pathology Score Assessment

Post-Xenium PAS-stained slides were used to perform a semi-quantitative assessment of tubular lesion score in kidney samples across time points by a blinded, board certified renal pathologist. Tubular lesion severity was graded on a scale of 0 to 4 across 8–10 fields of view selected within the deep cortex and corticomedullary junction. The average score was calculated to represent each sample. The tubular injury features considered included (1) epithelial atrophy (thinning, loss of apical cytoplasm, open lumen, reduced/absent brush borders on PAS staining); (2) tubular necrosis; (3) interstitial edema with mononuclear infiltrates. Semi-quantitative thresholds for all injury scores were as follows:

Injury score	0	1	2	3	4
Injury Level	0-10%	10-25%	25-50%	50-75%	>75%

For fibrosis quantification, Sirius Red staining was performed on sections from the same tissue samples used in this study. High resolution images were captured using a brightfield microscope at 20x magnification and image analysis was performed using QuPath (version 0.6.0). The kidney tissue area was delineated using the wand tool. Color deconvolution was performed to separate the Sirius Red signal and the SR-positive area was identified using pixel classification based on color-specific intensity threshold. The final percentage of interstitial fibrosis was calculated as:

$$\text{Intersitial fibrosis } (\%) = \frac{\text{SR Area}}{\text{Total kidney section Area}} \times 100$$

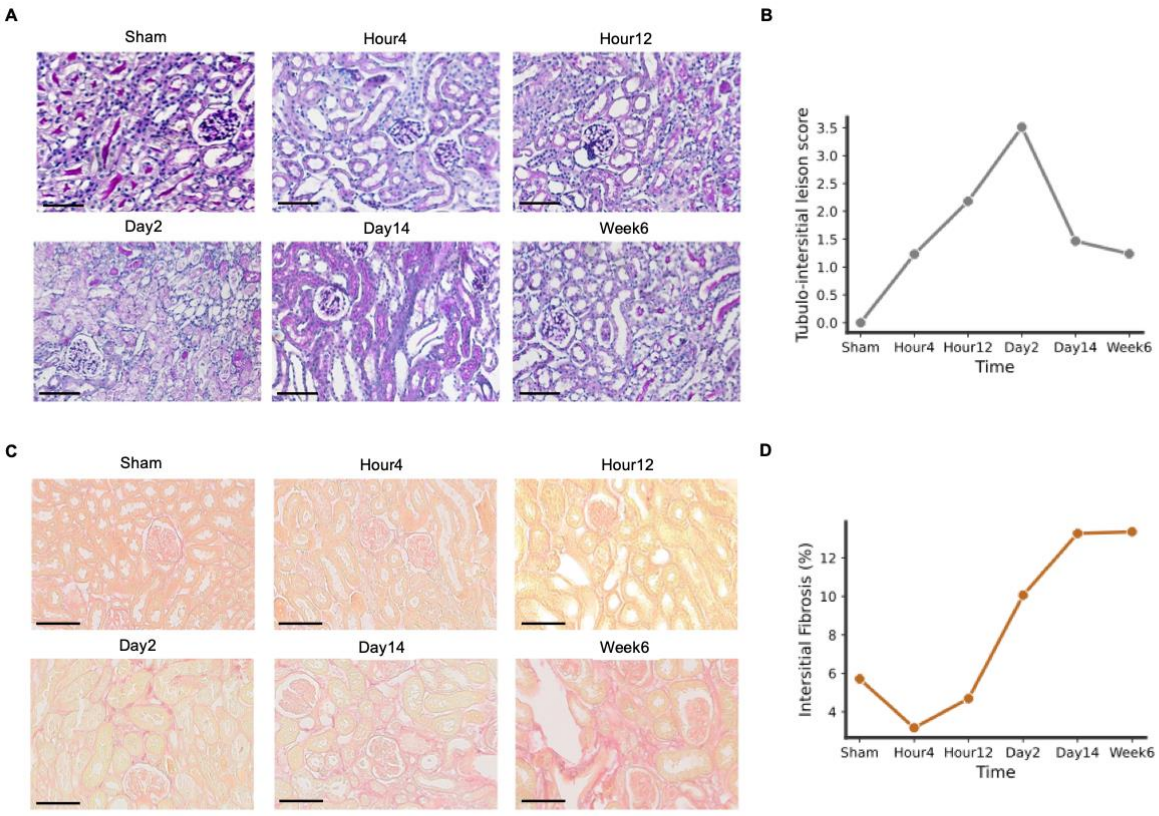

Response Figure 10. **A.** Representative Periodic acid-Schiff staining images over IRI time course. Scale bar: 40 μm. **B.** Quantified tubular lesion scores across IRI time course. **C.** Representative Sirius Red staining images over IRI time course. **D.** Quantified fibrosis scores across IRI time course.

4. Although the study design is inherently longitudinal, time-course investigations are not comprehensively performed. Time-course analyses of gene expressions and cellular interactions can provide valuable insights on the dynamism of the system. This trajectory analysis is crucial for understanding the dynamic progression of cellular states over time, particularly in the context of AKI and its transition to chronic kidney disease (CKD).

Response: Thank you for the suggestion to include additional time-course analysis taking advantage of our longitudinal data. We have added new analyses focused on cell-type colocalization and ligand-receptor interactions across multiple time points. More details on the rationale of these analyses can be found in our response to **Reviewer 2 questions 6–7**. For the longitudinal cell-type colocalization analysis, we have added the **Main Fig. 4D** and **Supplementary Fig. 7** to demonstrate the interaction hubs across the IRI time points. For the longitudinal LR analysis, we have revised **Main Fig. 6A** to quantify the LR co-expression dynamics across IRI time course and visualized the spatiotemporal signaling activities across time points (**Supplementary Fig.11**).

Additionally, we performed a spatial trajectory analysis of proximal tubule cell subpopulations. Unlike conventional pseudotime ordering of single-cell data, we implemented an algorithm which incorporates both transcriptomic data and spatial coordinates to map PT cells between consecutive time points. This approach enables us to identify the ancestors and descendants of distinct PT cell states in real experimental time, offering valuable insights into their transitions and potential fates during AKI to CKD transition. The revised manuscript includes a detailed description of this trajectory analysis in the Results section under "**Spatiotemporal mapping reveals distinct fates of proximal tubule cells**".

5. The interactions of fibroblasts with other cell types are extensively discussed in this work. However, this cell type is vaguely defined in the literature and other cell types can be mislabeled as fibroblasts. What markers were used to label this cell type? How can they be distinguished from pericytes? In figure 2D, PAS images and spatial transcriptomics data are overlaid to validate cell type annotation but this image does not include fibroblasts. Demonstrating these cells in the PAS images provides a clear evidence about their histologic identity.

Response: Thanks for highlighting the importance of accurately defining fibroblasts and distinguish them from other cell types. Consistent with the recent work by Kuppe et al. (PMID: 3317633), the fibroblast cluster in our study refers to extracellular matrix (ECM) producing cells and was annotated based on high expression of collagen markers, including *Col1a1, Col1a2*, ect. We grouped together pericytes and smooth muscle cells and annotate this cluster based on marker gene *Tagln, Acta2, Myh11 and Notch3*. We visualized their spatial distribution in a sham mouse kidney and observed that pericytes/SMC were mainly surround capillaries and small blood vessels while fibroblasts were found in the interstitial spaces of both the cortex and medulla region (**Response Figure 11**).

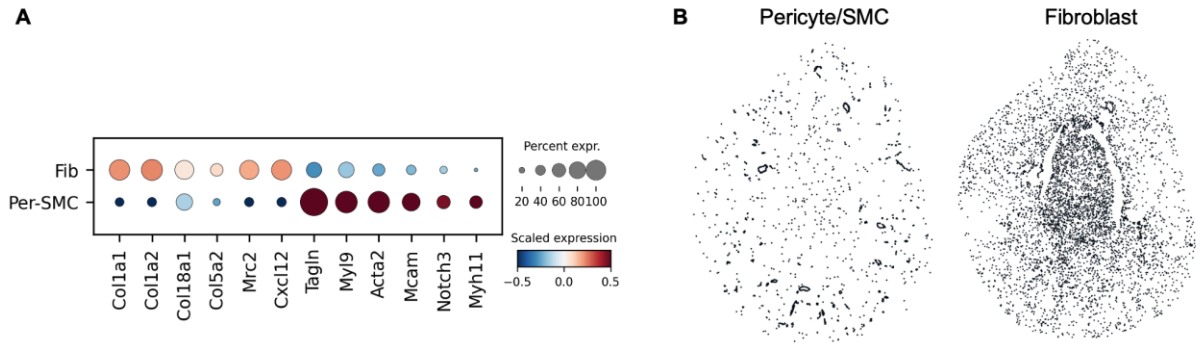

Response Figure 11. A. Scaled marker gene expression in fibroblast and pericyte/SMC cluster of Xenium data. **B.** Spatial distribution of fibroblast and pericyte/SMC in a control

We appreciate the suggestion to include histological validation of fibroblast annotation. We have updated **Main Fig. 2D** to include a PAS representative image of fibroblast cells. To demonstrate the histologic identity of fibroblast, we also selected different regions and showed that our annotated fibroblast cells exhibit elongated shape

distributed within the interstitial space between tubules (**Response Figure 12**).

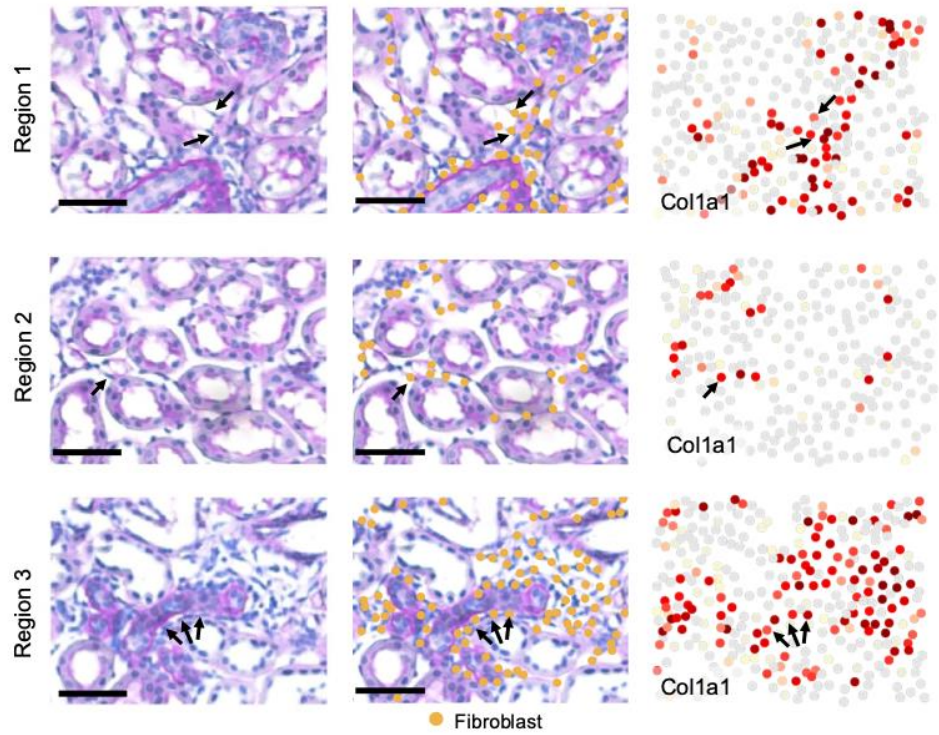

Response Figure 12. Representative PAS images overlayed with fibroblast annotations and marker expression.

6. Although the study presents extensive data on gene expression, there is limited functional validation of the findings. Experimental confirmation of the roles of identified processes would strengthen the conclusions.

Response: In the revised manuscript, we have incorporated two panels of experimental figures to validate the findings from our data analysis. We added immunostaining data to validate the ligand-receptor interaction analysis between FR-PTC and immune cells, FR-PTC and fibroblasts (Main **Fig. 6B-C**).

7. Minor points: a) in some cases the figures are not cited in the text in appropriate order. For instance Figure 2D is cited before 2A and so on. Additionally, some parts of the figures are not cited.

Thank you for pointing out the inconsistencies in figure citations. We apologize for this oversight. We have revised both the figure order and the corresponding references in the manuscript to ensure they are cited in the correct sequence. We have also removed any redundant figures that did not directly contribute to the main text.

b) The second paragraph of Results: Please provide SD or SE for the correlation indices.

We thank the suggestion of adding SE of the correlation indices. We now modified our original paragraph to include the calculated SE for the correlation within each replicate and with bulk RNA-seq data.

c) In line 96, referring to a correlation coefficient of r = 0.66 as a “high” correlation may be misleading. This is equal to an r^2 of 0.44 and a more accurate description would classify this correlation as moderate.

Thank you for your comment. We agree that the correlation coefficient of r = 0.66 would be more accurately described as "moderate" rather than "high." We have revised the manuscript accordingly.

Below is our revised manuscript:

Our results demonstrated a strong correlation in detected transcript counts for each gene across technical replicates at each time point (r=0.99±0.00) (Supplementary Fig.1B). Furthermore, a comparative analysis with bulk RNA sequencing data, focusing on of commonly detected genes also confirmed a moderate correlation (r=0.59± 0.04) (Supplementary Fig. 1E). Taken together, these data reflect the high quality and reliability of the Xenium spatial data generated in this study.

Reviewer #4 (Remarks to the Author):

This study by Xuanyuan et al. from Humphreys lab investigates the progression from acute kidney injury (AKI) to chronic kidney disease (CKD) in mouse, emphasizing changes in cellular composition and molecular interactions within the kidney. The Humphreys lab is a pioneering group in the field of single-cell and single-nucleus RNA sequencing (sc/snRNA-seq) and spatial transcriptomics of the kidney.
In this study they used advanced spatial transcriptomics platforms—Xenium for high-resolution single-cell data and Visium for whole transcriptome analysis—the authors examined over one million cells from 12 mouse kidneys across six stages of injury and repair. They identified 20 major kidney cell populations and mapped out distinct cellular neighborhoods. By analyzing ligand-receptor interactions, they revealed critical pathways involved in failed repair, chronic inflammation, and fibrosis, particularly in proximal tubule cells, fibroblasts, and immune cells.
The integration of Xenium and Visium data is a standout feature of the study and represents a pioneering effort in kidney research, marking the first time these two technologies have been used side by side to elucidate the progression from AKI to CKD.
The paper is well-written and easy to follow.

Thank you for these positive comments.

Overall, my comments and suggestions are as follows:

Major comments:
-Please provide the creatinine values as a plot, similar to the BUN data, at different time points in Figure 1.

Response: Thank you for your valuable feedback and for your interest in our study. We appreciate your suggestion to include creatinine values to reflect the kidney injury levels across time. However, we regret to inform you that we do not have creatinine measurements. We only measured BUN levels and have no serum leftover. However, in previous studies from our lab that utilized the same bilateral IRI model of AKI, we have directly measured GFR by the FITC-sinistrin method, and confirmed a substantially reduced GFR after IRI (PMID: 34853151).

-Please include the fibrosis score and tubular atrophy assessment, as determined by a pathologist, at different time points in Figure 1.

Response: Thank you for your suggestion. We have performed two histopathologic assessments: 1) Quantification of tubular lesion score on PAS-stained images. 2) Quantification of fibrosis score on Sirius red-stained images. Please see the updated **Main Fig. 1B-E** and detailed description of the methodology in the '**Pathology Score Assessment**' subsection of the Methods.

-Please explain how to choose the 300 genes for the panel for Xentium? Did you use your previous snRNA-seq dataset as reference to choose? Expand on the validation of the 300-gene panel—were any additional pilot studies done to ensure it covered all cell types and relevant disease states?

Response: Thank you for your thoughtful comment. The majority of the genes included in our panel were manually selected based on snRNA-seq dataset using our interactive data visualization website (http://humphreyslab.com/SingleCell/). To validate that our selected gene panel effectively covers all major cell types, we subsetted our snRNA-seq dataset to include only the selected 300 genes. We performed clustering analysis to assess whether the reduced gene set could still identify major cell types present during AKI. We have added a **Supplementary Fig. 12** which demonstrated the clustering result of reduced snRNA-seq dataset and the dotplot showing the marker gene expression (**Response Figure 13**). We have updated the Methods section of the manuscript to provide a more detailed explanation of the gene selection process.

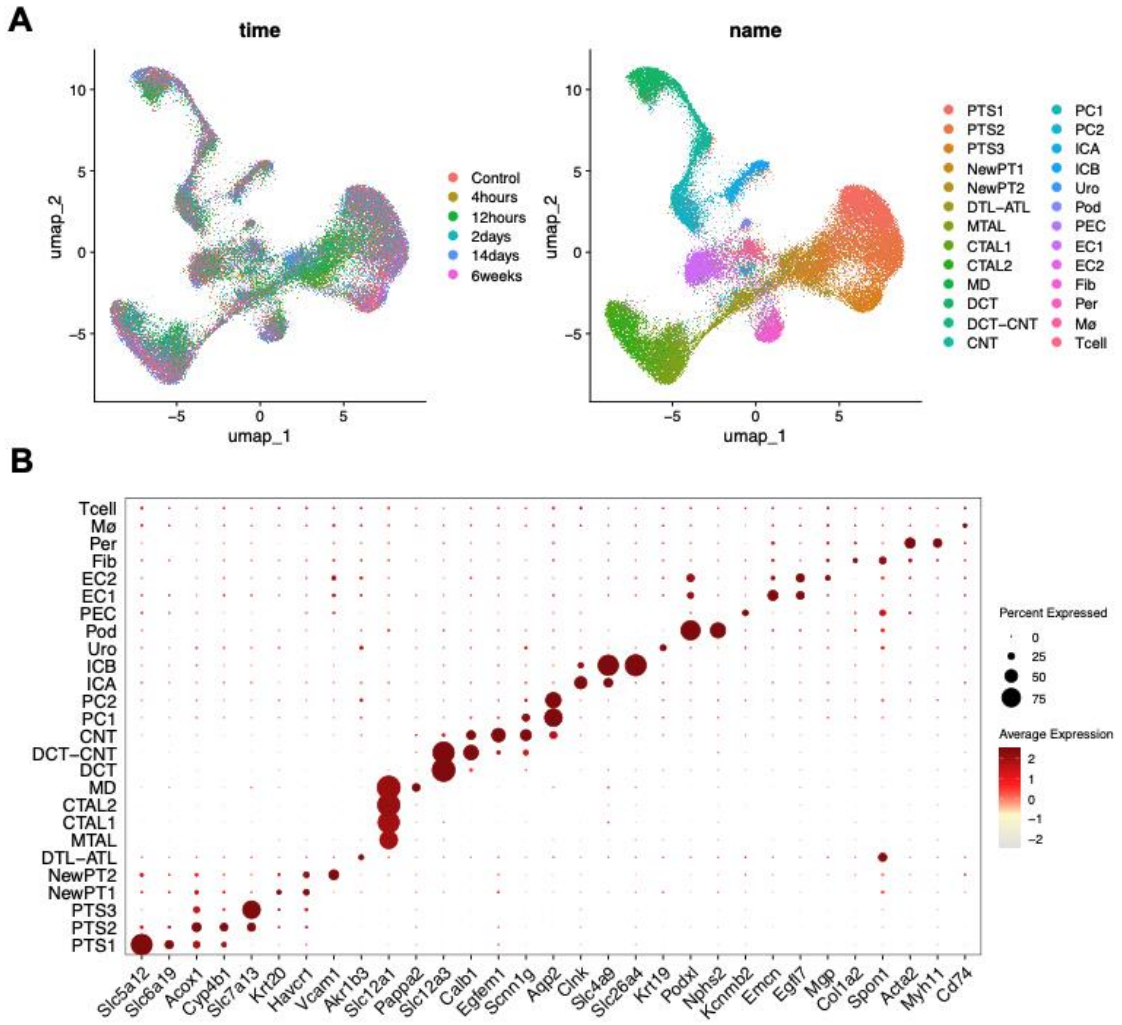

Response Figure 13. A. UMAP projection of snRNA-seq data clustered using 300 gene panel. **B.** Dotplot showing the marker gene expression across cell types using reduced snRNA-seq data.

-Please explain why Baysor was specifically chosen for segmentation. It would be helpful to provide a comparison between Baysor, Cellpose, Stardist, and Deepcell, demonstrating why Baysor is the most suitable method for your dataset.

Response:

1. Baysor is a cell segmentation tool that optimizes cell boundaries based on the joint likelihood of transcriptional composition and cell morphology. This allows Baysor to leverage transcript data alongside DAPI imaging to achieve more accurate cell boundary estimation. Baysor can also incorporate a prior segmentation mask (generated from DAPI nuclei segmentation), with an adjustable hyperparameter, prior-segmentation-confidence, which controls how much the algorithm adheres to the prior segmentation. In contrast, tools such as Cellpose, StarDist, and DeepCell primarily rely on DAPI segmentation.

2. To address your suggestion for a comparative analysis, we have included supplementary information (**Supplementary Note 1 and Supplementary Fig. 15**) that visualizes the segmentation results of the mentioned methods: XeniumNuclei, Baysor (with Prior), Cellpose, StarDist, DeepCell. We remapped the transcripts to cells segmented using the different algorithms and quantified the number of transcripts assigned to cells using each method. Our results demonstrate that Baysor effectively balances the retrieval of transcripts and achieves good separation of cell. All other nuclear segmentation methods resulted in significantly fewer transcripts (**Response Figure 14**).

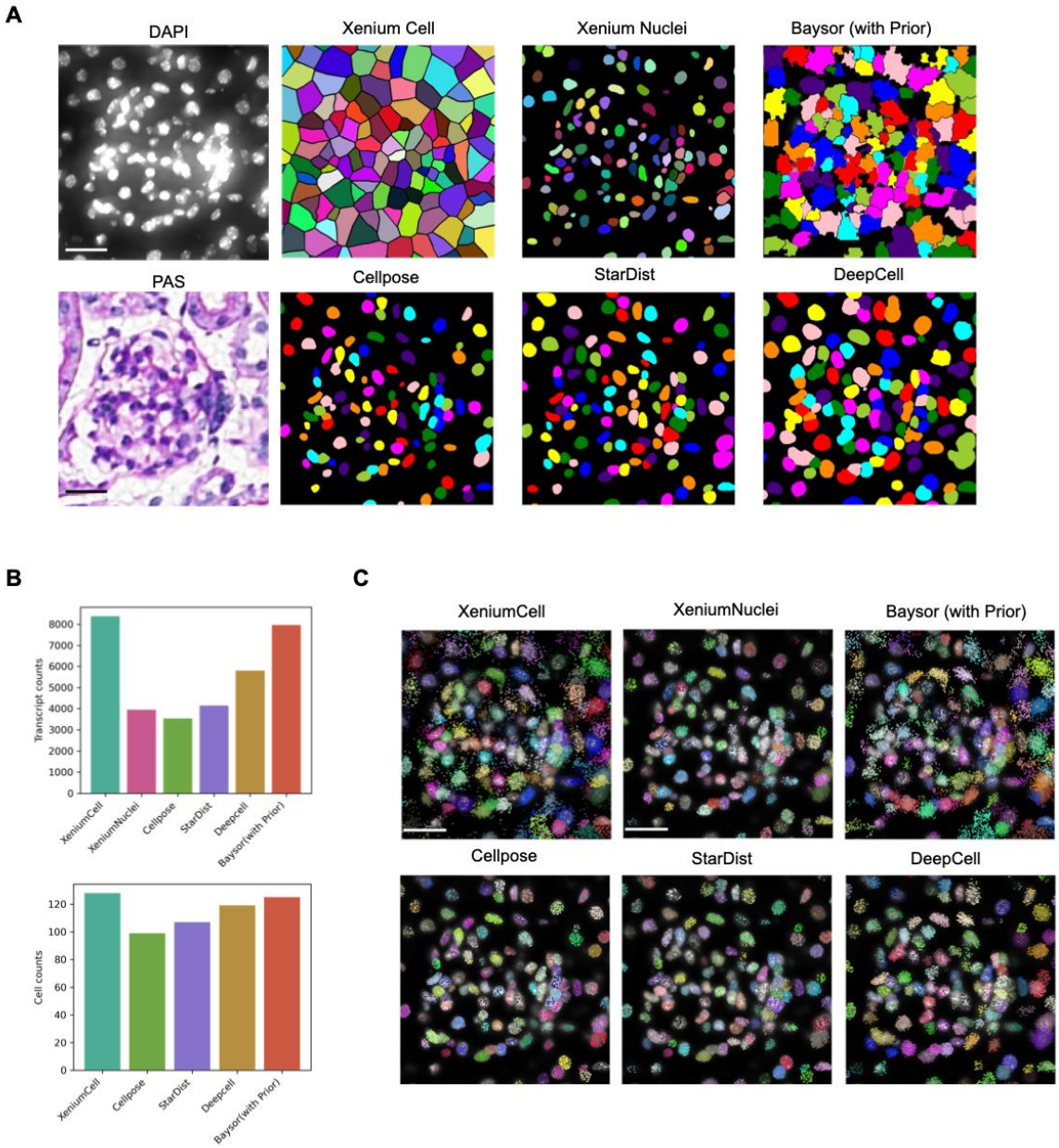

Response figure 14. **A.** Comparison of segmentation results. **B.** Comparison of retrieved cell counts and transcript counts. **C.** visualization of retrieved transcripts after remapping to segmented cells using different algorithms. Transcripts are colored by their corresponding segmented cell ID. Xenium (nuclei): default Xenium nuclei segmentation; Baysor (with Prior): Baysor segmentation using Xenium nuclei segmentation as a prior. Scale bar: 20 um

- It appears that macula densa cells were not clearly identified in the Xenium data, as the prediction score for these cells (SF 1G) is low. You included Pappa2 as a marker for macula densa in the panel. Could there be an issue with the probe? Could you please explain the potential reason for this low identification score?

Response: We thank this comment regarding the identification of MD cells in our Xenium dataset. Xenium provides eight probes targeting Pappa2 gene and we verified their target binding sites of these probes using the Integrative Genomics Viewer (IGV) (**Response Figure 15A)**.

We visualized the Pappa2 transcript distribution in Xenium cells using Xenium Explorer (10x Genomics). We found that Pappa2 transcripts were predominantly localized in the JGA as expected, and only a few cells expressed this marker. This observation is consistent with the rarity of the MD cell type (**Response Figure 15B**).

We performed subclustering analysis within the thick ascending limb (TAL) cluster, where Pappa2 gene has stronger expression. However, we were unable to separate MD cell cluster from the TAL cluster based on Leiden clustering. The limitation is likely due to the 300 gene targets detected by Xenium and the small population size of MD cells (**Response Figure 15C)**.

To summarize, the low identification score for MD cells in our dataset may be due to both the limited marker selected for this cell type and the low abundance of MD cells.

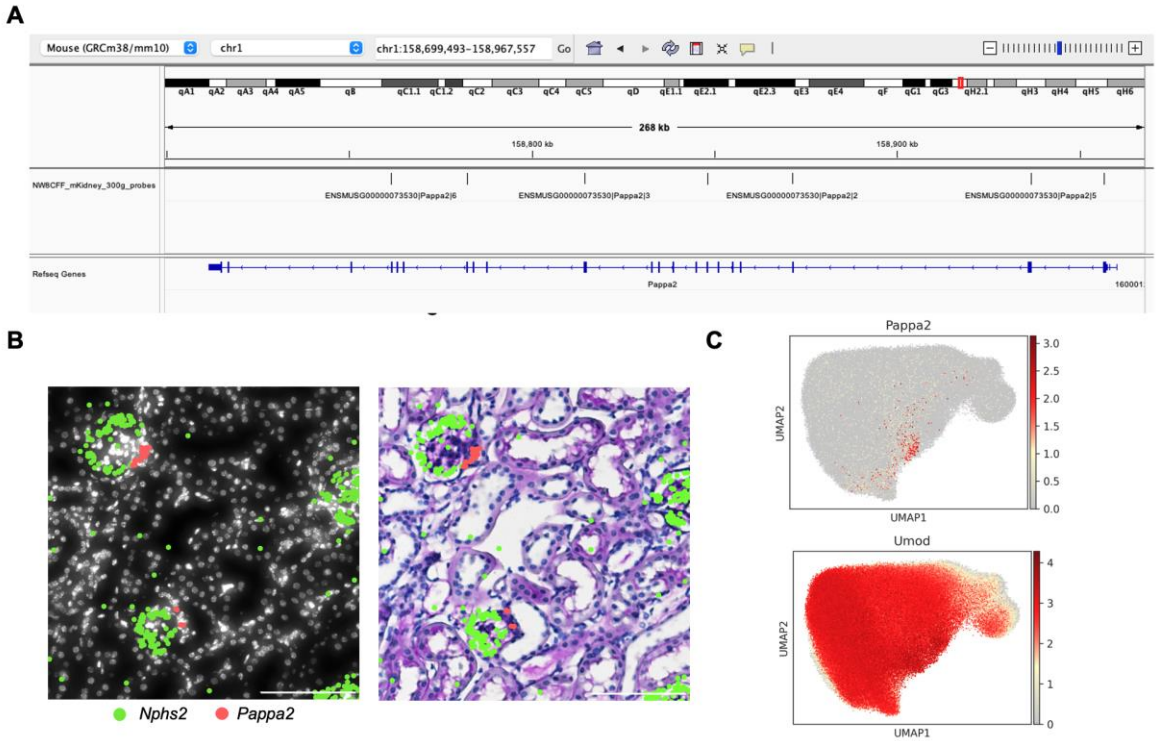

Response Figure 15. A. Pappa2 probe mapping on genomic locations using IGV. **B.** Spatial distribution of Pappa2 and Nphs2 transcript in Xenium data (Week6 sample). **C.** *Pappa2* expression in TAL subcluster.

- Please provide an integration of the Xenium and snRNA-seq datasets. Currently, the study presents a heatmap of the prediction scores, but it would be beneficial to integrate the snRNA-seq and Xenium spatial data and present it as a UMAP, showing marker genes in the integrated dataset. This integrated dataset would offer more comprehensive insights and be highly useful for the study.

Response: Thank you for your suggestion to integrate the Xenium spatial data with the snRNAseq data. We have utilized a canonical correlation analysis (CCA)-based integration workflow to co-embed both datasets into a shared UMAP space (**Response Figure 16**). We have added a new supplementary figure (**Supplementary Fig. 3**) that shows the integrated UMAP projection of the two datasets and displayed the expression patterns of key marker genes.

We have included a detailed description of the integration workflow in the Method section.

Xenium and snRNA-seq data integration

To integrate the Xenium spatial transcriptomics data and snRNA-seq data, we first identified the overlapping genes present in both datasets. The integration process was carried out in two key steps. In the first step, we aimed to correct for batch effects originating from the differences between the two platforms. Both datasets were normalized by total count and log-transformed. We then applied Seurat's canonical correlation analysis (CCA) via the ALLCools Python package using the top 100 principal components (PCs) for feature selection. In the second step, we removed the batch effects caused by the varying IRI disease conditions across samples using harmony integration. After correcting for platform and condition-based batch effects, we co-embedded the datasets by constructing a neighborhood graph and visualized them using UMAP based on the 15 nearest neighbors in the integrated PCA space.

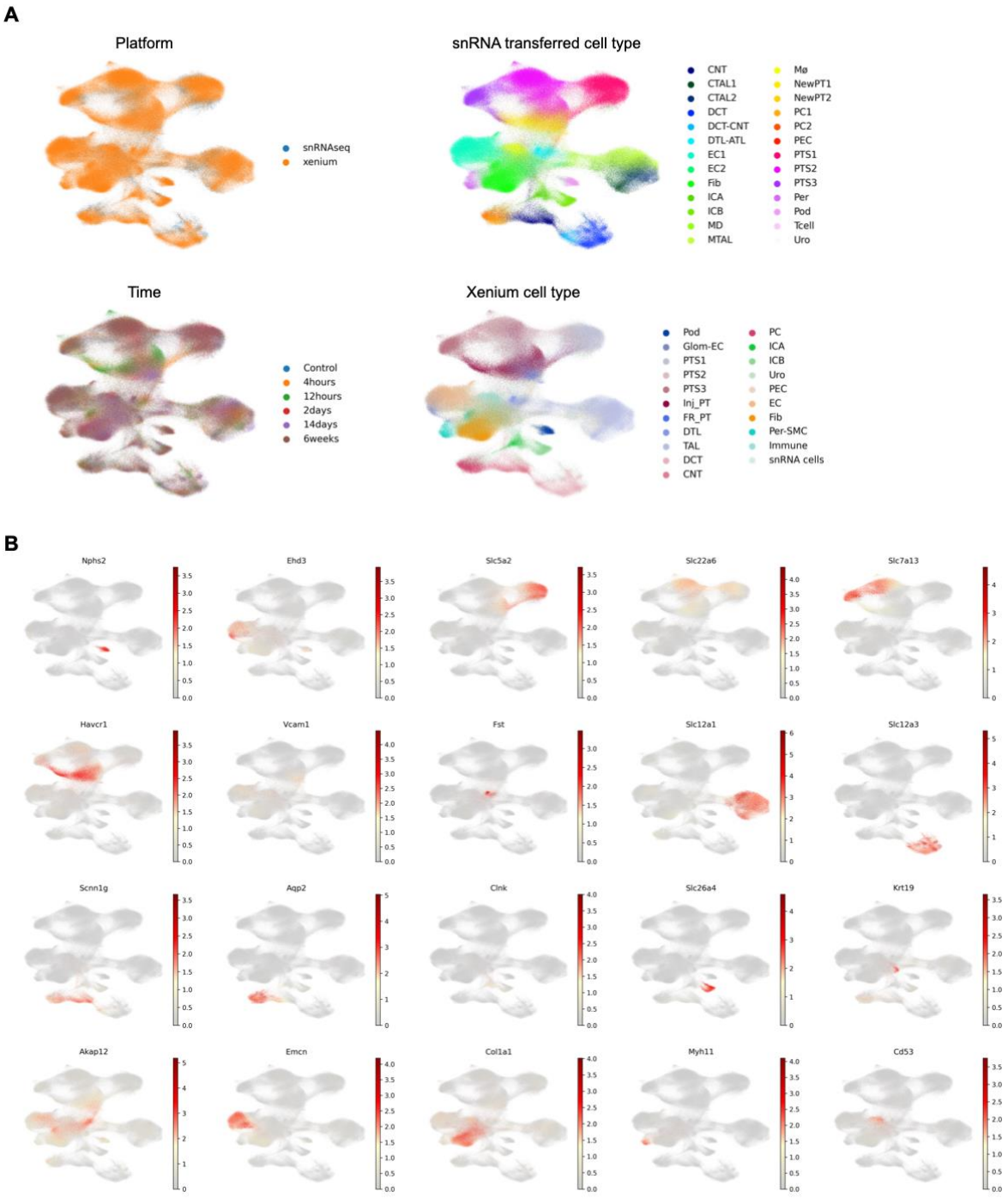

Response Figure 16. A. UMAP showing the co-embedding of integrated Xenium and snRNA-seq datasets. **B.** Expression of cell type marker genes on the co-embedded UMAP space.

- It would be helpful to rename the CNs 1-9 with specific names based on the predominant cell types forming them, such as renaming CN1 as "glomerular niche," etc. This would make it easier to follow and understand the context of each neighborhood.

Thank you for the suggestion. We have revised the CN names to add descriptions reflecting their overall cell composition. Similar revision has been applied to the CN label in Visium data. Please see the revised **Main Fig. 4A, Fig. 5E**.

- Similar to the CNs, the clusters in Figure 5 obtained from Visium could be renamed based on the predominant cell types contributing to their formation, rather than using numbers. This would enhance clarity and make the clusters easier to interpret.

Thank you for the suggestion. We have revised the CN names to add descriptions reflecting their overall cell composition. Please see the revised **Main Fig. 4A,** and **Fig. 5E**.

-The text mentions that Visium clusters were manually adjusted to match the spatial organization of CNs identified in Xenium data. Providing more details on how this manual adjustment was performed would improve transparency. Were certain criteria or algorithms used for this process, and how were the adjustments validated to ensure accuracy?

Response: We appreciate your feedback regarding the manual adjustment of Visium clusters to match the spatial organization of cell neighborhoods identified in Xenium data. We acknowledge that manual adjustments can introduce biases and may lack reproducibility. We have utilized an alternative method to transfer labels to Visium spots based on their neighborhood cell-type composition similarity. We have updated all the downstream analysis results in Visium neighborhood related analysis. Please refer to **Response Figure 6A** or the revised main text result section "**Molecular characterization of tissue cell neighborhoods through integration of whole transcriptome spatial data**" for the updated findings. This approach ensures the robustness and reproducibility of our analysis.

We have added a method subsection to describe the label transfer process. Below is the method:

Cell neighborhood label transfer from Xenium to Visium data

We constructed cell composition matrices for both the Xenium and Visium datasets by matching their spatial scales. For the Xenium data, we calculated local cell type frequencies within a 55-micron radius around each cell, corresponding to the size of a Visium spot. For the Visium data, we deconvoluted each spot to estimate the proportion of each cell type present based on reference Xenium data. We performed PCA on combined matrix to obtain a joint embedding of the two datasets. To match the Visium spot to Xenium cell neighborhood, we identified the top 20 nearest neighbors given a Visium spot based on the joint embedding. We assigned the cell neighborhood label to

each Visium spot based on majority voting among the labels of these nearest Xenium cells. To demonstrate the robustness of our label transfer, we performed a leave-one-out cross-validation on the Xenium data. In each iteration, one Xenium cell was left out, and the remaining cells were used for integration with the Visium data to predict the neighborhood label for the left-out Xenium cell. The overall prediction accuracy was 0.84, indicating a high level of confidence in our ability to recreate the structural organization identified in Xenium at the Visium resolution.

- I believe it would be beneficial to perform a cell colocalization analysis, using a package such as CellTrek, on the clusters/CNs from the Visium data, as well as on the Xenium data. For example, I am particularly interested in seeing the neighboring cells of CN4. This analysis would provide a better understanding of regional cell density and population dynamics in the mouse kidney.

Response: Thank you for the suggestion on cell colocalization analysis. We have carefully considered your recommendation to use CellTreck for colocalization analysis on Visium dataset. However, CellTrek is designed to map the single-cell data back to the spatial location through co-embedding sc data with Visium data. While this method can estimate the spatial distribution of cell types in higher resolution, it does not provide an accurate representation of actual cell neighborhood composition and cell colocalization patterns. In our case, integrating Visium data with reference snRNA-seq data using CellTrek resulted in overestimation of macrophages and T cells. This observation is consistent with our findings in the deconvolution section of the manuscript. Given this, we performed the colocalization of cell types to demonstrate the cell-type interaction dynamics using Xenium data.

1. To investigate the cell type co-localization dynamics, we performed colocalization analysis in Xenium data. We defined a proximity threshold of a 55-micron diameter circle to assess the interaction frequency between two cell types within this window. The colocalization z-score was used to quantify the strength of interaction frequency between cell types relative to a randomized distribution. Our analysis validated that cells enriched within specific neighborhoods also exhibited high co-localization scores. For example, in the collecting duct region (CN5), enriched cell types such as ICA, ICB, PC, and CNT consistently showed high co-localization scores (z-score > 20) across all IRI time points. Similarly, in the fibro-inflammatory neighborhood (CN7) at day 14, we observed high co-localization scores between FR-PT cells and fibroblasts (z-score = 30), FR-PT cells and immune cells (z-score = 24), and fibroblasts and immune cells (z-score = 27) (**Response Figure 7**).

2. As requested, we also performed co-localization analysis between different cell neighborhoods. However, since each CN is defined by its unique local cell composition within 55 diameter area, the colocalization scores between cells from different CNs were generally low (**Response Figure 17**). This is because cells within the same CN are more likely to interact due to their physical proximity and shared local environment, whereas cells from different CNs are separated by compositional boundaries.

Response Figure 17. Co-localization between each CN across IRI time points.

3. To specifically address your interests in CN4—the injured proximal tubule neighborhood — we isolated all cells belonging to CN4 from Xenium dataset and calculated the colocalization scores between each pair of cell types within CN4 across all IRI time points. We then aggregated the colocalization scores to average the interaction patterns over time. Our findings revealed significant colocalization between Inj-PT cells, fibroblasts and immune cells within this neighborhood (**Response Figure 18**).

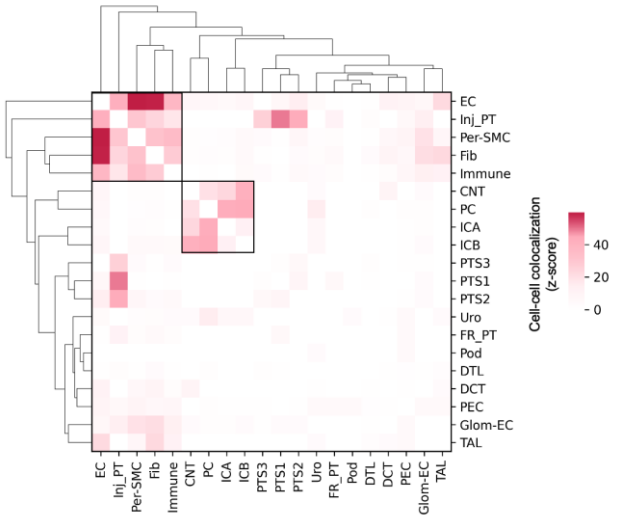

Response Figure 18. Cell-cell colocalization heatmap within injured proximal tubule

- One of the most interesting aspects of the study is the identification of “inj-PT” and “FR-PT” cells. These seem similar to the populations identified by the Susztak lab (PMID 39048792) as “iPT_VCAM1+” and “iPT_HAVCR1.” The question is whether the

cells identified in the present study are indeed analogous to those previously described in humans, as mentioned. A side-by-side comparison would be useful in clarifying this.

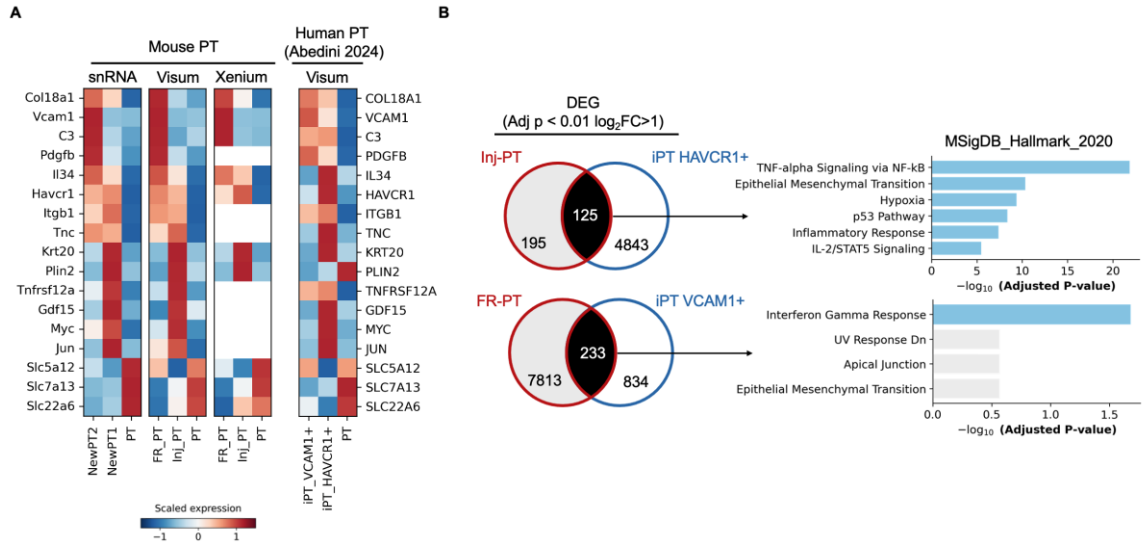

Response Figure 19. A. Comparison of marker gene expression across identified PT cell states in mouse snRNA-seq (Kirita 2020), mouse Visium and Xenium (this study) and human Visium dataset (Abedini 2024). Genes not included in Xenium panel were left blank. **B.** Venn diagrams showing differentially expressed genes (DEGs, log2FC>1) of PT states common to mouse and human Visium dataset. Gene ontology analysis was performed using these shared genes. In the GO analysis of genes common between FR-PT (mouse) and iPT VCAM1+ (human) non-significant terms are depicted in gray.

We appreciate the reviewer's question regarding the analogy between the altered PT cell states identified in our study and those previously described by the Susztak lab. Our analysis demonstrates that the inj-PT cells in our mouse model closely correspond to the iPT_HAVCR1+ cells described in human studies. Both populations exhibit significant upregulation of injury markers (*Havcr1*), and pro-inflammatory genes (*Gdf15, Jun*), (**Response Figure 19A**). We performed Gene Ontology (GO) enrichment analysis on the shared upregulated genes between mouse inj-PT cells and human iPT_HAVCR1+ cells. The results revealed enrichment in pathways such as TNF-alpha signaling via NF-κB and hypoxia response. These pathways indicate activation of stress responses and an inflammatory state in the PT cells of both species (**Response Figure 19B**).

The comparison between FR-PT cells in mice and iPT_VCAM1+ cells in humans also revealed similarities. We identified 233 upregulated genes that overlap between mouse FR-PT cells and human iPT_VCAM1+ cells. Both populations show upregulation of adhesion molecules such as VCAM1 and CD44. The increased expression of these adhesion molecules indicates a pro-fibrotic phenotype, potentially facilitating cell-cell adhesion and extracellular matrix (ECM) accumulation. However, GO analysis of shared

upregulated genes only highlighted the enrichment of the interferon-gamma response pathway (**Response Figure 19B**).

The difference between FR-PT cells in mice and iPT_VCAM1+ in human could be attributed to several factors. FR-PT cells were identified in our BIRI mouse model during the transition from AKI to CKD, whereas the human data represents established CKD disease. The divergent gene expression profile may reflect the heterogeneity of VCAM1+ epithelial cells and distinct maladaptive repair mechanism of injured PT cells in mice versus human.

Additionally, is the “inj-PT” population more associated with disease or inflammatory status?

Based on the gene expression profiles and pathway analysis, we conclude that the “Inj-PT” cell population is more closely associated with an inflammatory status resulting from ischemia/reperfusion injury. We have found that high proportion of the upregulated genes are related to inflammation (I*tgb1, Tnfrsf12a, Tnc*) and oxidative stress responses (*Fosl2, Klf6, Jun*). Similarly, pathway analysis results are also associated with the acute inflammatory response (**Response Figure 19B)**.

Do “inj-PT” and “FR-PTC” cells interact with each other, and does “inj-PT” potentially develop from “FR-PTC”? This could be explored further through colocalization analysis, which could help answer these questions. Moreover, a trajectory analysis, particularly at the spatial level, would provide valuable insights into the progression and relationship between these cell types.

Through colocalization analysis, we found ‘Inj-PT’ and ‘FR-PT’ cells display strong colocalization score at day 14 and week 6 **(Response Figure 7)**.

After subclustering of PT cells in Xenium dataset, we identified seven distinct PT subpopulations: three healthy PT segments (Healthy S1, S2, S3), three injured PT segments (Inj S1, S2, S3) and one failed-repair PT cell population (FR-PT) (**Response Figure 20**).

To explore the progression and relationships among altered PT cells, we conducted trajectory analysis using SpaTrack. Unlike conventional pseudotime ordering of single-cell data, SpaTrack employs optimal transport algorithms and leverages both transcriptomic data and spatial coordinates to map the spatiotemporal dynamics of cells. This approach allows us to infer the ancestors and descendants of different PT cell states, providing insights into the cell states transition over time. Shortly after injury (sham -> 4 hours -> 12 hours), we observed a clear shift from healthy PT cells to inj-PT cells. Over time, some Inj-PT began to recover and revert to healthy states (hour12 -> day2). However, by day14 post-injury, a significant proportion of Inj-PT cells transitioned into the FR-PT cell population, which persisted up to six weeks post-injury (**Response Figure 21A**). The observed transitions suggest that Inj-PT cells can develop into FR-PT cells, indicating a maladaptive repair process which can lead to chronic kidney damage.

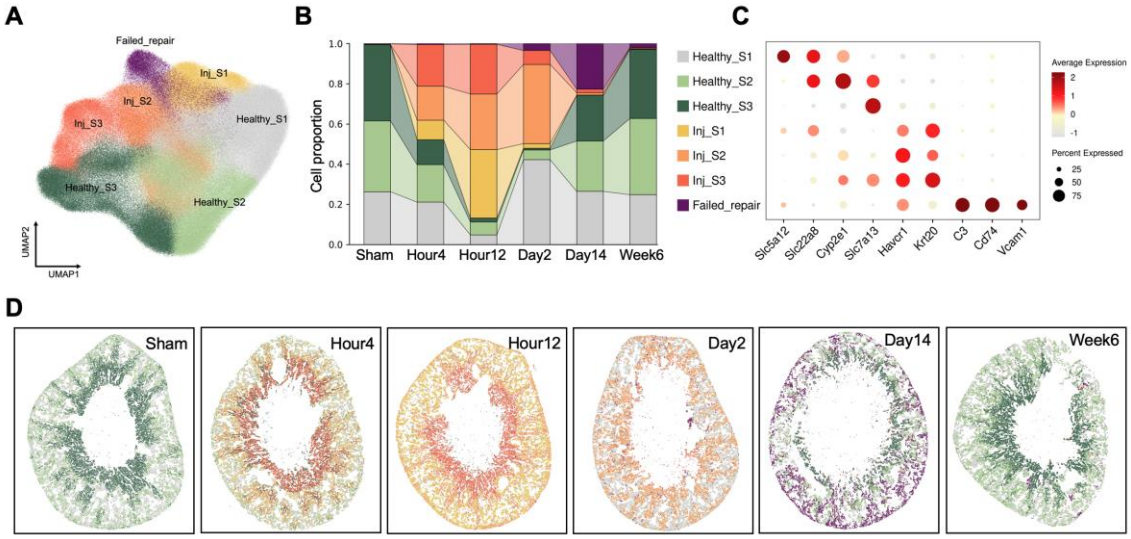

Response Figure 20. A. UMAP displaying PT cell subpopulations in Xenium. **B.** Temporal composition of PT cell states. **C.** Marker gene expression of identified PT cell states. **D.** Spatial distribution of PT cell states across IRI time course.

To further explore the fate of Inj-PT cells, we focused on cells from day 2 post-injury and classified them based on their state at day 14 (**Response Figure 21B)**:

1. Stable Healthy PT Cells: Healthy PT cells at day 2 that remain healthy at day 14.
2. Recovering Injured PT Cells: Inj-PT cells at day 2 that recover to a healthy state by day 14.
3. Maladaptive Injured PT Cells: Inj-PT cells at day 2 that progress to become FR-PT cells by day 14.

This classification enabled us to compare the molecular profiles of inj-PT cells with different outcomes (**Response Figure 21C**). We performed differential gene expression analysis on the Inj-PT cells with different fates. Recovering injured PT cells showed higher expression of genes including *Cxcl12*[1], which plays a role in facilitating repair following I/R injury through maintaining mitochondrial homeostasis. Other upregulated genes *Haao*, *Kynu* and *Hmgcs2* involved in kynurenine pathway and ketogenesis have also been associated with renoprotective effects[2,3]. Maladaptive injured PT cells exhibited high expression of genes including *Serpine1*[4], *Cd44*[5] and *Klf5*[6]. The elevated expression of these pro-fibrotic and adhesive genes indicates that maladaptive Inj-PT cells are contributing to the creation of a fibrotic microenvironment. This environment not only facilitates their own transition into FR-PT cells but may also exacerbate tissue fibrosis.

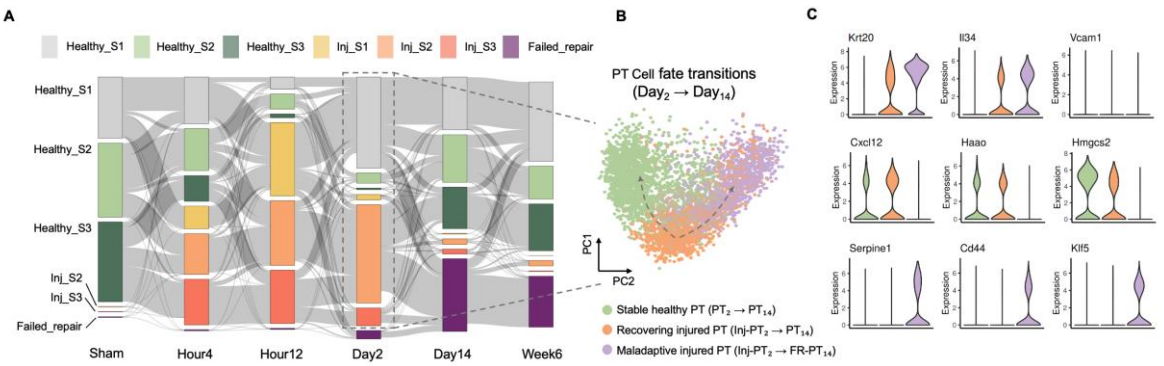

Response Figure 21. A. Sankay diagram displaying the transition between PT cell states in Xenium data. **B.** PCA embedding of the PT cell at day2. **C.** Violin plot showing marker genes of PT with different cell fates.

We have added a new result section "**Spatiotemporal mapping reveals distinct fates of proximal tubule cells**" to include the trajectory analysis of PT subpopulations.

Reference:

1. Yakulov TA, Todkar AP, Slanchev K, et al. CXCL12 and MYC control energy metabolism to support adaptive responses after kidney injury. Nat Commun. 2018;9(1):3660. doi:10.1038/s41467-018-06094-4
2. Gui Y, Palanza Z, Gupta P, et al. Calponin 2 regulates ketogenesis to mitigate acute kidney injury. JCI Insight. 8(21):e170521. doi:10.1172/jci.insight.170521
3. Späth MR, Hoyer-Allo KJR, Seufert L, et al. Organ Protection by Caloric Restriction Depends on Activation of the De Novo NAD+ Synthesis Pathway. J Am Soc Nephrol JASN. 2023;34(5):772-792. doi:10.1681/ASN.0000000000000087
4. Ghosh AK, Vaughan DE. PAI-1 in tissue fibrosis. J Cell Physiol. 2012;227(2):493-507. doi:10.1002/jcp.22783
5. Matsushita K, Toyoda T, Akane H, Morikawa T, Ogawa K. CD44 expression in renal tubular epithelial cells in the kidneys of rats with cyclosporine-induced chronic kidney disease. J Toxicol Pathol. 2024;37(2):55-67. doi:10.1293/tox.2023-0111
6. Liu Y, Wang Y, Xu C, et al. Activation of the YAP/KLF5 transcriptional cascade in renal tubular cells aggravates kidney injury. Mol Ther. 2024;32(5):1526-1539. doi:10.1016/j.ymthe.2024.02.031

- The comparison of different deconvolution methods was excellent and much needed. Thank you for including that analysis.

Response: Thank you for recognizing the value of our comparison of different deconvolution methods. In response to feedback from other reviewers who expressed concern that this benchmarking might detract from the primary biological focus, we have moved these results to the **Supplementary Note 2**. We appreciate your understanding.

- Does the pseudo-Visium data allow for a more accurate comparison of Xenium and

Visium, or is it primarily a validation tool? More explanation on its purpose would strengthen the reader's understanding of this method.

Response: Thank you for your comment. The purpose of generating pseudo-Visium data is to enable a quantitative comparison between the Xenium and Visium platforms. By mimicking the spatial resolution and gene expression patterns of Visium, pseudo-Visium data allows us to assess the degree of alignment between the two datasets. Specifically, we assess the spatial gene expression correlation by aggregating Xenium data for cells that are physically located within the same Visium spot and comparing it to the gene expression profile of that spot in the Visium data. As illustrated in **Supplementary Fig. 8A-D**, this approach demonstrates the alignment of data between the two platforms.

Our ultimate goal is to transfer cell neighborhood labels identified in the high-resolution Xenium dataset to Visium. A high degree of concordance between the datasets increases confidence in leveraging Visium's deep transcriptomic data to further characterize these neighborhoods.

We have added the purpose of this quantitative comparison in the result (line 1339-1341).

Overall, we demonstrated strong concordance in spatial gene expression patterns between Xenium and Visium, supporting the use of Visium's broader transcriptomic data to enhance the characterization of cell neighborhoods identified by Xenium

-Please consider expanding the description of BANKSY's spatial clustering process, as readers unfamiliar with this method might benefit from more details.

Response: Thank you for your suggestion regarding an expanded description of the BANKSY spatial clustering process. In our initial approach, we utilized BANKSY clustering on imputed day 14 data to refine cell type annotations before performing ligand-receptor analyses. However, as we revised the manuscript to extend ligand-receptor analysis across all time points, we realized that re-annotating with BANKSY would introduce inconsistencies with our original cell type annotations. To maintain consistency in cell type definitions, we decided not to rely on BANKSY clustering in our study. Instead, we imputed the Xenium dataset using the reference snRNA-seq data and use our original cell type annotations when performing the LR analysis. We appreciate your understanding.

-Pathway analysis might benefit from integrating additional tools like IPA (Ingenuity Pathway Analysis) to explore upstream regulators or causal networks.

Response: We have used decoupleR, which utilized univariate linear model (ULM) to infer upstream TF regulators for the CN7 (fibro-inflammatory niche) (**Response Figure 22**). We have added the regulatory network to the **Main Fig. 5G** and **Supplementary Fig. 9D**.

We have added the interpretation of GRN in the result section “Molecular characterization of tissue cell neighborhoods through integration of whole transcriptome spatial data”.

To better understand the transcriptional drivers of the fibro-inflammatory niche, we inferred the upstream transcription factor (TF) activities using the Visium spatial data. Key TFs, including Hivep2, Nfat5 and NFκB, which have been previously linked to the transition of tubular cells into failed repair (FR) state[1,2], were significantly upregulated within this niche. Spi1 (PU.1) is a critical regulator of macrophage polarization, which has been demonstrated to promote their differentiation into a pro-fibrotic M2 phenotype[3]. Notably, Runx2, a transcription factor associated with pulmonary fibrosis[4] and cardiac-fibroblast proliferation[5], also emerged as a prominent regulator in this niche. RUNX2's regulatory network modulates the expression of target genes such as Col1a1, Mgp, and Mmp2, all of which are key players in extracellular matrix remodeling and fibrosis progression. Taken together, these findings suggest a tightly interconnected transcriptional program that aligns the functions of FR-PT cells, fibroblasts, and immune cells, collectively shaping the fibro-inflammatory niche.

Reference:

1. Ledru, N. *et al.* Predicting proximal tubule failed repair drivers through regularized regression analysis of single cell multiomic sequencing. *Nat. Commun.* **15**, 1291 (2024).
2. Muto, Y. *et al.* Epigenetic reprogramming driving successful and failed repair in acute kidney injury. *Sci. Adv.* **10**, eado2849 (2024).
3. Qian, F. *et al.* The transcription factor PU.1 promotes alternative macrophage polarization and asthmatic airway inflammation. *J. Mol. Cell Biol.* **7**, 557–567 (2015).
4. Mümmler, C. *et al.* Cell-specific expression of runt-related transcription factor 2 contributes to pulmonary fibrosis. *FASEB J. Off. Publ. Fed. Am. Soc. Exp. Biol.* **32**, 703–716 (2018).
5. Ebrahimighaei, R. *et al.* Combined role for YAP-TEAD and YAP-RUNX2 signalling in substrate-stiffness regulation of cardiac fibroblast proliferation. *Biochim. Biophys. Acta BBA - Mol. Cell Res.* **1869**, 119329 (2022).

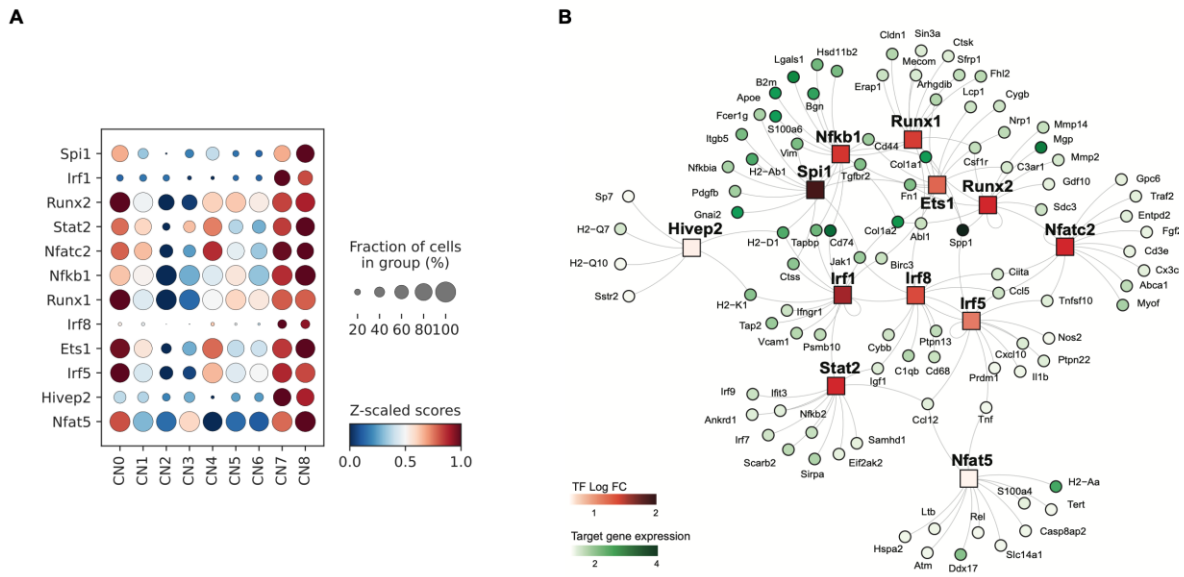

Response Figure 22. A. Dotplot visualizing top transcription factor activities identified in Visium fibro-inflammatory niche (CN7). **B.** Graph network of top significant transcription factors (adjust p < 1e-20) and target genes. The complete table of significantly predicted TFs is provided in Supplementary Data 5.

-The description of image registration between Visium and Xenium data could benefit from more clarity. Consider adding more detail on how manual landmark selection was performed to ensure reproducibility.

Response: Thank you for this comment. In response, we have included **Supplementary Figure 13** to demonstrate workflow of the two-step image registration. When choosing landmarks, we relied on distinct morphological features such as the glomeruli structure or vascular structures. We have updated the Method section to include these details. To ensure reproducibility, we have published the transformation matrix between Visium spot coordinates and Xenium cell coordinates in our code reproducibility GitHub repository (https://github.com/TheHumphreysLab/IRI_Xenium_Visium/blob/main/Analysis/4_Xenium_Visium_integration/1_visium_xenium_registration.ipynb).

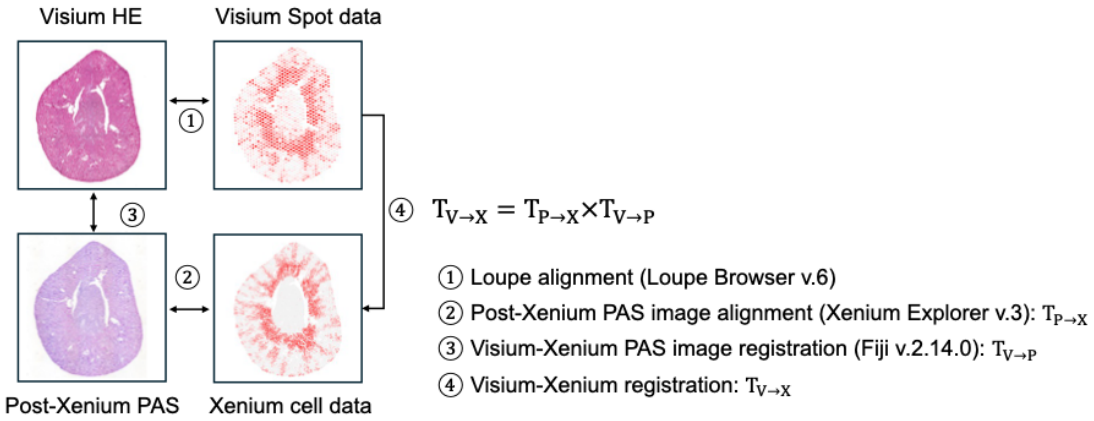

Response Figure 23. Visium to Xenium registration workflow.

(1). Loupe alignment was performed to align the high-resolution HE images to Visium spot coordinates (V). (2). The Xenium PAS image was aligned to the Xenium DAPI image using the Xenium Explorer software. The transformation matrix $T_{P\to X}$ maps the PAS image to the Xenium cell coordinates (X). (3). The Visium HE image was registered to the Xenium PAS image. This derived a transformation matrix ($T_{V\to P}$). (4). For the final registration, the transformation matrices from the two steps were combined to map Visium spots to Xenium coordinate system.

- While the focus is on IRI-induced kidney injury, a brief comparison of the molecular characteristics of the CN7 (Cluster 7) with those observed in other models of kidney disease (e.g., diabetic nephropathy) could provide additional context. Are these CNs specific to IRI, or might they be found in other kidney injury models? Such a discussion could broaden the relevance of the findings.

Response: We have extended our discussion of the neighborhood identified in this study with other spatial transcriptomic datasets including Polonsky (2024) (mouse IRI) and Abedini (2024) (human CKD) **(Supplementary Fig. 9E, F).** We quantified the average expression levels of neighborhood-derived DE genes across cell types identified in both mouse and human datasets. In mouse IRI datasets, the highest CN7 gene signature activity was observed in injured PT cells, fibroblast and macrophages. Similarly, in human CKD datasets, CN7 activity was enriched in mesangial cells, fibroblasts, parietal epithelial cells (PECs) and endothelial cells of lymphatic vessels, albeit with a weaker activity in injured PT cells. Moreover, diseased samples (day28 post-IRI kidneys in mice and CKD kidneys in humans) consistently exhibited significantly elevated CN7 activity compared to control samples. These findings support the cross-species conservation of CN7 signature as a key fibro-inflammatory axis likely driving the AKI to CKD progression.

We appreciate the suggestion to compare our findings with other kidney disease like diabetic nephropathy model. However, publicly available spatial transcriptomic datasets for diabetic nephropathy are currently limited.

- While the study provides strong evidence for ligand-receptor interactions at the transcriptional level, these findings have not been validated at the protein level. It is crucial to confirm that the upregulated LRIs are functionally active in the tissue microenvironment. They should validate the identified LRIs through immunohistochemistry (IHC) or immunofluorescence (IF) staining at least for some of them such as IL34, Csf1r, etc. This would help confirm the spatial localization and interaction of proteins such as TGF-β, PDGF, IL34 and WNT ligands in the tissue, thereby providing stronger evidence for their role in fibrosis and inflammation.

Response: Thank you for the suggestion regarding the experimental validation of our findings. As co-localization of IL-34 in VCAM1+ tubule cells has already been demonstrated by Gerhardt et al[1]. (Figure 5E), we have chosen to focus on validating additional ligand-receptor pairs identified in our study (**Main Fig. 6A**). We identified the *Icam1-Itgb2* interaction as a significant pair mediating communication between FR-PTF and immune cells. We performed immunofluorescence staining on day 14 post-injury kidney sample and observed the co-localization of ICAM1 on VCAM1+ FR-PT cells and ITGB2 on F4/80+ macrophages. Please check our updated **Main Figure 6** and result description.

Reference:
1. L.M.S. Gerhardt, J. Liu, K. Koppitch, P.E. Cippà, A.P. McMahon, Single-nuclear transcriptomics reveals diversity of proximal tubule cell states in a dynamic response to acute kidney injury, Proc. Natl. Acad. Sci. U.S.A. 118 (27) e2026684118, https://doi.org/10.1073/pnas.2026684118 (2021).

Minor comments:
-Fig. 2A: Please add color labels for each cell type in the figure.

We have added the color labels in Main Fig. 2A.

-Please present a UMAP grouped by samples, along with a plot showing the distribution of each sample within each cell type.

We have added this in **Supplementary Fig. 1F-G**.

-Please include PEC in Supplementary Figure 2.

We have added spatial distribution of PEC in Sham in **Supplementary Fig. 2**.

- Line 535: There is no Figure S9C in the manuscript. Did you mean Figure S1G?

We apologize for the oversight. We have corrected the figure citation to refer to updated **Supplementary Fig. 10A**.

Reviewer #4 (Remarks on code availability):

The code was reviewed, and STIM provided clear instructions for installation and usage.
The code for generating the figures and conducting the overall analysis was also checked and found to be comprehensive.

We thank the reviewer's comment on code availability. Due to the extensive number of figures generated during the revision process, we have moved the reproducible code to GitHub (https://github.com/TheHumphreysLab/IRI_Xenium_Visium) with detailed descriptions for better accessibility and readability.

Reviewer #5 (Remarks to the Author):

I co-reviewed this manuscript with one of the reviewers who provided the listed reports. This is part of the Nature Communications initiative to facilitate training in peer review and to provide appropriate recognition for Early Career Researchers who co-review manuscripts.

REVIEWER COMMENTS

Reviewer #1 (Remarks to the Author):

The authors made great efforts to address my concerns, which I appreciate, but I still have some questions.

1) We have demonstrated a high correlation between our imputed gene expression patterns and the detected gene expression using the genes shared between the Xenium and snRNA-seq data (Response Figure 1A, Supplementary Fig. 10A).

The shared genes are the ones used for imputation. Therefore, the imputed and actual expressions are expected to present high correlation. I would suggest the authors ran some bootstrapping, excluding a percentage of genes from the imputation algorithm and testing the correlation on that subset. A possible study would be the minimum percentage of tissue-specific genes necessary to obtain a satisfactory correlation. This could be a very useful result for future researchers when designing their panel. It would be possible to estimate the adequate proportion of cell marker genes and other genes of interest for a particular study.

We thank the reviewer for this comment. We have now evaluated the imputation using a cross-validation strategy. In this approach, the cell-type marker genes in Supplementary Fig. 10A were excluded during imputation. We have updated the heatmap using this refined method to better illustrate the imputation accuracy (Response Figure 1A).

We agree that panel design is crucial for optimizing cell-type annotation accuracy in imaging-based spatial transcriptomics studies. However, determining the minimal percentage of tissue-specific genes necessary for satisfactory correlation was not the primary goal of our study, as correlation metrics alone do not fully capture panel-design efficacy due to the inherent variations in gene expression levels and spatial distribution. To directly address the reviewer's question, we conducted an additional evaluation where we excluded known cell-type marker genes (Response Figure 1A, Supplementary Fig. 10A) as validation genes and performed gene imputation using only the top differentially expressed (DE) genes at varying thresholds (top 5 and top 10 DE genes per cell type). Our results show that using the top 10 DE genes per cell type (112 genes after duplicate removal) achieved comparable imputation accuracy (mean PCC = 0.53) relative to the full set of 279 genes (mean PCC = 0.54) (Response Figure 1B).

To optimize panel design, computational methods have been specifically developed (PMID: 38273415; PMID: 38408997) to balance cell-type classification accuracy and minimize platform bias. We want to clarify that imputation correlation alone is not a definitive criterion for effective panel design, as a well-optimized panel must consider both biological relevance and technical constraints beyond imputation performance alone.

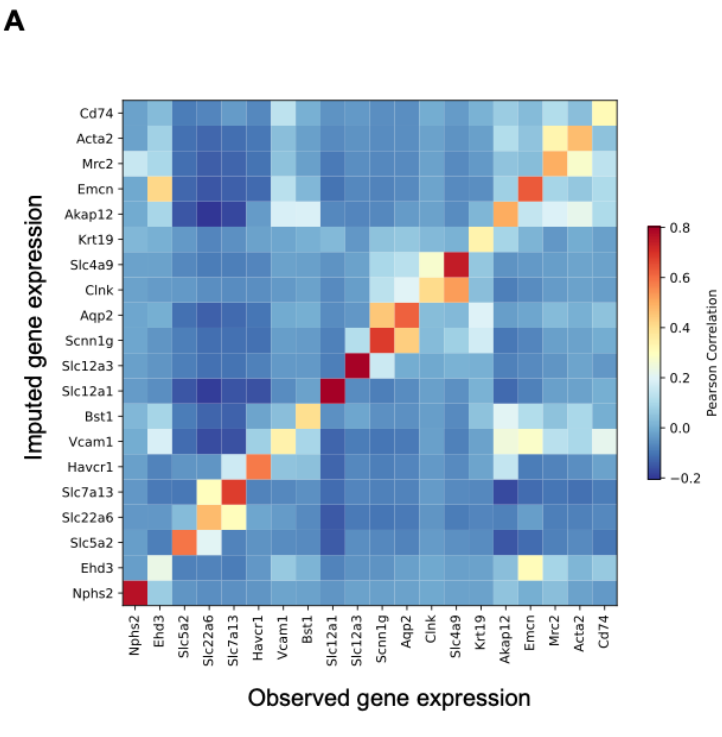

Response Figure 1. **A.** Correlation between observed expression and imputed expression. Genes were dropped from Xenium during the integration process. **B.** Boxplots of root mean square error (RMSE) and Pearson correlation coefficient (PCC) for imputation performance using different numbers of genes. The top 5 cell-type-specific gene set contains 57 genes, while the top 10 cell-type-specific gene set contains 112 genes after duplicate removal.

2) I appreciate the effort in explaining the spatial localization of specific markers. I want to emphasize that I believe receptor-ligand analysis is one of the technical frontiers of spatial technologies and is poised to provide unique insight into injury mechanisms and potential therapeutic targets. I appreciate the authors pushing the envelope in this particular front. But for that very reason, a precise description of the method and its limitations is essential. The list I provided was not extensive. I suggest the authors provide a supplemental table with the location of these markers in the spatial technologies. Also, and appropriate evaluation of the imputation mechanism would bring confidence into this important result.

We acknowledge the limitation of current imputation algorithms and we have added the limitations of imputation-based LR inference to the discussion. However, we do not rely only on the imputed results from Xenium. To mitigate the risk of false positives, our experimental design incorporated an adjacent Visium dataset to cross-validate our ligand-receptor findings. As demonstrated in Figure 6, the signaling activities observed in the Visium data closely align with those predicted from the Xenium imputed dataset. We have also used immunostaining to validate one of the predicted LR interactions. To further increase the confidence of our result, we have added more figures to

Supplementary Figure 10 visualizing the imputed gene expression in Xenium, along with the observed gene expression in Visium (Response Figure 2).

Our supplementary data 6 provides a comprehensive list of ligand-receptor genes inferred from Xenium imputed dataset and supplementary data 7 details the top significant ligand-receptor pairs identified within each cell neighborhood using Visium data. We have visualized the spatial distribution of observed signaling pathways in supplementary fig 9 and quantified their signaling activity across different cell neighborhoods. We believe the cell-cell communication results in Visium and the supplemental resources directly addresses concerns regarding imputation performance.

We appreciate the reviewer's suggestion for a more rigorous evaluation of the imputation mechanism. However, benchmarking various imputation algorithms is beyond the primary scope of our study. Extensive benchmarking studies have already been published (PMID: 35577954, PMID: 40082609) and both these works suggest SpaGE as the optimal method for imputation.

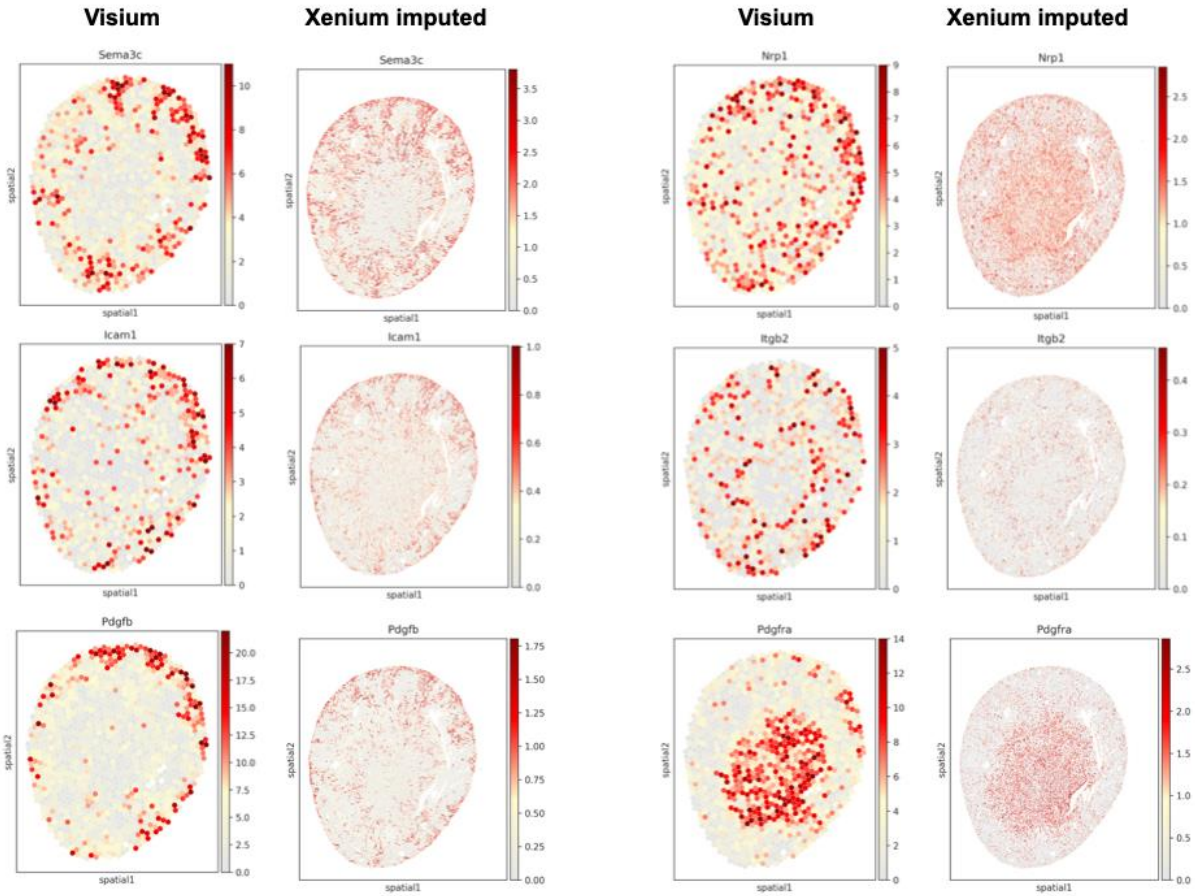

Response Figure 2. Comparison between Xenium imputed gene expression and Visium observed gene expression at day14 sample.

3) The authors made a fantastic effort on the code availability. Detailed code is fundamental for science reproducibility, and the authors took a leap in the right

direction. There are still a few steps missing in the analysis; for instance, the preprocessing of the file Xenium_all.h5ad is not clearly identified, and there is no script for the package commot. I apologize to the authors if I come across as nit-picky. This package is relevant because its default distance in visium is 500 microns, and therefore, contact interactions have to be evaluated critically, especially in a tissue such as a mouse kidney with very small structures. I want to be clear that the authors are ahead of the curve in code availability, and while more details would be desirable, the repository is at a stage where the effort is yielding diminishing results. Thank you for your effort in making the code available.

We appreciate your feedback about the processed anndata object and we have now uploaded the Xenium data object to Figshare (https://figshare.com/articles/dataset/Xenium_IRI/28761695/1?file=53543495, See Data Availability).

The script for COMMOT analysis is in our GitHub repo: https://github.com/TheHumphreysLab/IRI_Xenium_Visium/blob/main/Analysis/6_Ligand_receptor/Figure6C-H.ipynb where we documented the distance threshold to calculate the cell-cell communication (dis_thr=100). We also included the distance in the method section.

Reviewer #1 (Remarks on code availability):

I believe the repository is a good resource as currently presented.

Reviewer #2 (Remarks to the Author):

I want to thank the authors for their answers and improvements to the manuscript. I have no further comments.

Reviewer #3 (Remarks to the Author):

The authors have fully addressed my questions and I do not have additional concerns.

Reviewer #4 (Remarks to the Author):

The authors have made substantial improvements in the revised manuscript in response to reviewer comments. I appreciate the extensive efforts they have undertaken, including clarifying methodological choices, incorporating additional validation experiments, and strengthening integration with previous literature. Several of my concerns have been adequately addressed; however, there are still areas that could

be further refined to enhance clarity, rigor, and overall impact.
My comments are as follows:

-It would be beneficial to validate the identified neighborhoods using an alternative method such as CellCharter (PMID: 38066188). While the authors have used a cell-based approach for neighborhood identification, incorporating an embedding-based method for validation would help assess whether alternative approaches identify any biologically relevant structures that may have been missed by the current method.

Thank you for this feedback. We have benchmarked two additional embedding-based neighborhood calculation approaches suggested by reviewer2 in the previous reviewer response document (Reviewer 2, Comment 3). To assess the consistency between the embedding-based method using CellCharter and our cell-based method, we compared the clusters generated by both approaches. We selected the number of clusters (n = 9) based on the cluster stability of CellCharter (Response Figure 3A). Our results indicate that most of the cell-based neighborhoods we identified were also recovered by CellCharter (Response Figure 3B). One unique neighborhood CellCharter identified is CellCharter_CN5, which consisted exclusively of TAL cells (Response Figure 3C). We also noticed that due to the limited feature space of only 300 genes, CellCharter's stability fluctuates as the number of neighborhoods increases (Response Figure 3A). This indicate that embedding-based method may not be the optimal approach to identify neighborhoods.

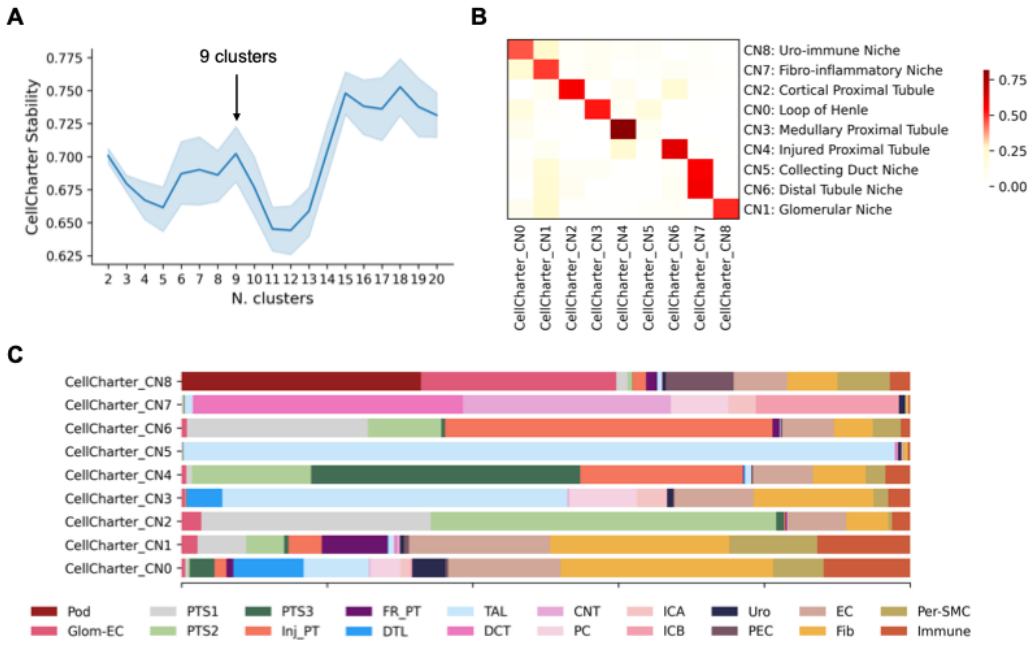

Response Figure 3. **A.** CellCharter cluster stability analysis across different cluster numbers. **B.** Comparison between cell neighborhood clusters identified using CellCharter and our method. Values indicate the proportion of cells within neighborhood annotated using our method that are classified into CellCharter neighborhood. **C.** Cell type composition across CellCharter identified neighorhoods.

-The identified transcription factors (TFs) require validation at the protein level. For instance, the claim that Runx2 and Spi1 are key transcriptional regulators driving fibrosis is based purely on inferred TF activity scores. Without further validation, these conclusions remain speculative. Please perform IHC or IF to validate the expression and spatial localization of these TFs and their roles in fibrosis.

We have now performed immunostaining to confirm the *Runx2* expression in nuclei of αSMA+ fibroblasts. We also observed *Runx2* expression in some tubular epithelial cells with lower intensity compared to fibroblasts. We have updated the Main Figure 5 to include this validation.

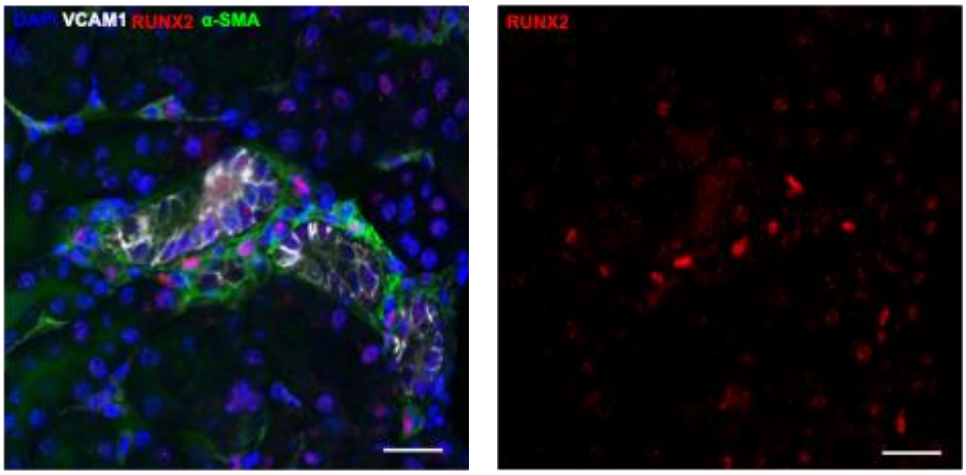

Response Figure 4. Immunostaining of VCAM1, RUNX2 and αSMA on day 14 BIRI kidney sample. Note that αSMA+RUNX2+ fibroblasts are close to VCAM1+ tubular epithelial cells. Scale bar: 20 μm.

-Please label the neighborhood names in the heatmaps of Figure 6 and Supplementary Figure 9 to improve interpretability.

Thank you for this comment. We have added the description of the neighborhoods to the corresponding figure legend to improve interpretability.

-Please include P-values in sections comparing cell-type frequencies, particularly in “Spatial transcriptomics accurately recovers cell type composition dynamics in IRI mouse kidney”, where different cell-type compositions are compared across time points. Adding statistical significance will strengthen the validity of these comparisons.

We thank the reviewer for this comment. We have now added the Adjusted *P* value < 0.05 to the main text. The P values were shown in Supplementary Fig. 4. Source data is also provided to strengthen the validity of the comparison.

Reviewer #4 (Remarks on code availability):

The code for generating the figures and conducting the overall analysis was reviewed

and found to be clear and comprehensive.

Reviewer #5 (Remarks to the Author):

I co-reviewed this manuscript with one of the reviewers who provided the listed reports. This is part of the Nature Communications initiative to facilitate training in peer review and to provide appropriate recognition for Early Career Researchers who co-review manuscripts.

Dear editorial team of *Nature Communications,*

This is a review of the "*Multimodal spatial transcriptomic characterization of mouse kidney injury and repair*" as an impartial referee.

This study employs advanced spatial transcriptomics techniques, specifically high-resolution Xenium and whole transcriptome Visium platforms, to analyze cellular dynamics in mouse kidneys across various stages of renal injury and repair. While the approach is promising and offers valuable insights into the cellular and molecular mechanisms underlying kidney injury, several limitations must be addressed to enhance the overall robustness and applicability of the findings:

1. **Limited Gene Panel:** The primary limitation of the exploited Xenium platform is its restriction to a panel of only 300 selected genes, which may not adequately capture the full transcriptome landscape necessary for a comprehensive analysis. This constraint could result in a major bias in the downstream analyses, particularly if key markers fall outside the selected gene panel. For instance, the insufficient mitochondrial markers in the Xenium panel may result in ignorance of a key component in the AKI pathogenesis. Additionally, the single-nucleus RNA sequencing (snRNA-seq) mentioned in the manuscript, neglects mitochondrial transcripts, which can constitute up to 50% of the total cellular transcriptome in kidney cells. Integrating the Xenium and Visium data and performing the downstream analysis based on the whole transcriptome data from Visium, not only the 300 gene set, can compensate this drawback.
2. **Overemphasis on Specific Cell Types**: An overemphasis on specific cell types and pathways might obscure other important contributors to the disease process, potentially limiting the overall understanding of AKI.
3. **Lack of Trajectory Analysis**: The omission of trajectory analysis is a significant oversight. This analysis is crucial for understanding the dynamic progression of cellular states over time, particularly in the context of AKI and its transition to chronic kidney disease (CKD).
4. **Limited Functional Validation**: Although the study presents extensive data on gene expression, there is limited functional validation of the

findings. Experimental confirmation of the roles of identified genes in kidney injury and repair would strengthen the conclusions.

5. **Misleading Correlation Interpretation**: In line 96, referring to the correlation coefficient of $r=0.66$ as a "high" correlation may be somewhat misleading. A more accurate description would classify this correlation as moderate.

In summary, while the study presents valuable insights into the cellular and molecular dynamics of kidney injury and repair, addressing these limitations will enhance the robustness and applicability of the findings. Thank you for considering my review.